August 1994

Fluid Targets for Heat Removal in Fusion Reactors

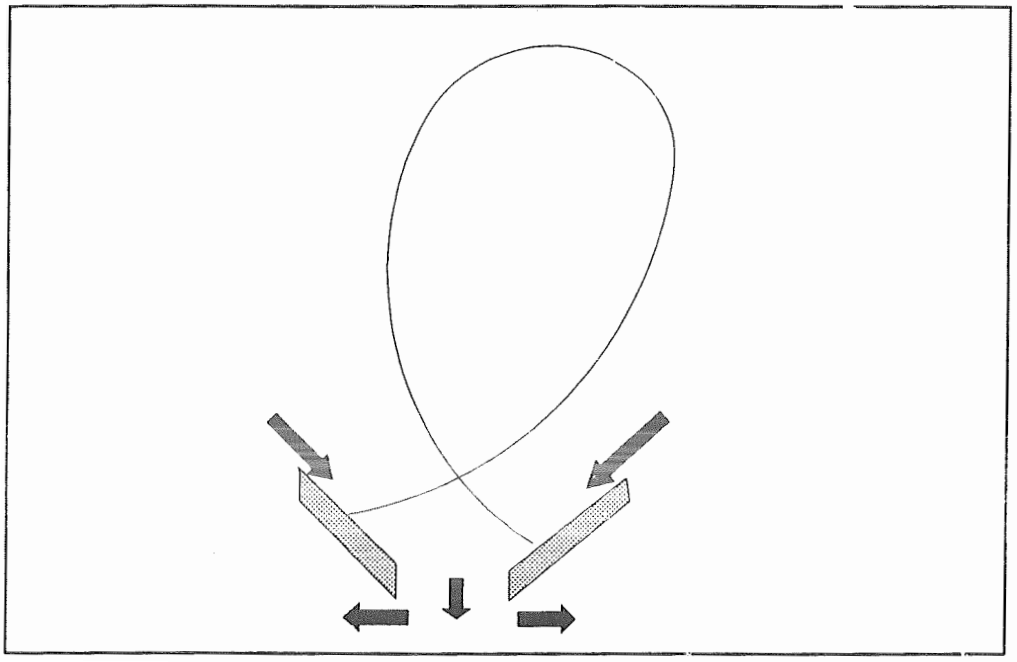

Interim report

J. Winter, V. Philipps (Editors)

Fluid Targets for Heat Removal in Fusion Reactors

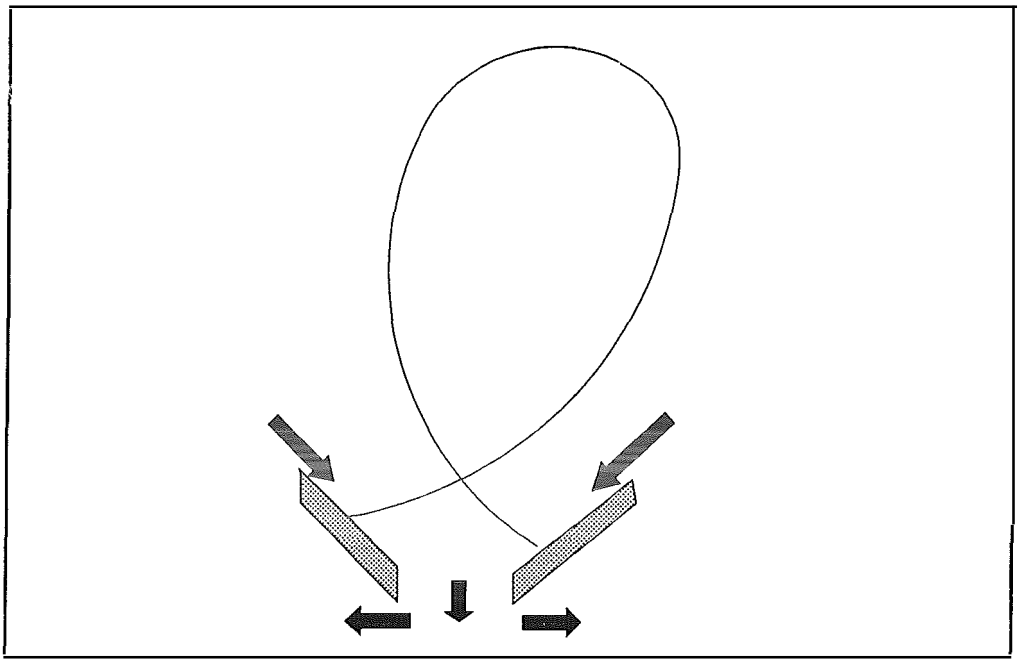

Interim report

J. Winter, V. Philipps (Editors)

List of authors

L. Binkele, Institut für Werkstoffe der Energietechnik 1

G. Breitbach, Institut für Werkstoffe der Energietechnik 1

P. Jung, Institut für Festkörperforschung

A. Kaleck, Institut für Plasmaphysik

W. Kohlhaas, Institut für Plasmaphysik

V. Philipps, Institut für Plasmaphysik

J. Winter, Institut für Plasmaphysik

Forschunszentrum Jülich GmbH
POB 1913
D- 52425 Jülich

Fluid Targets for Heat Removal in Fusion Reactors

0. Preface

Fluid targets, i.e. liquids or solids moving through the high heat flux zones, may be a way to solve the heat exhaust and erosion problems in fusion reactors. Some of the ideas are not new and are presented in the literature in widely scattered articles. Unfortunately, the discussion is often not detailed enough to judge their applicability. They have e.g. been addressed in the framework of the INTOR and ITER studies.

This report contains contributions of members of a study group constituted from scientists and engineers of different Institutes of KFA end of 1993. The group met a few times to discuss ideas and problems associated with the use of fluid targets for heat exhaust in fusion reactors. The starting point has been a proposal for a respective program on TEXTOR. The main aim of the group's work has been so far to identify critical questions warranting in depth studies in preparation of a potential experiment in TEXTOR. The treatment of the matter in these contributions is by now means complete and exhaustive but some important conclusions still can be drawn.

Reference to literature is made in the individual contributions where appropriate. In addition to these references a number of publications of general interest have been used and are listed in the appendix.

The contributions partly consist of summaries in english and copies of figures and viewgraphs in german which are selfexplaining in most cases.

1. General considerations (J. Winter)

The extraction of power from the high heat load components in a fusion reactor and their erosion are critical issues. The problems are unsolved, regardless of the magnetic configuration (tokamak / stellarator, divertor / limiter).

Most of present day's fusion devices operate with short plasma pulses of up to a few 10 seconds and employ solid fixed armor material which is adiabatically heated up. It does not allow heat removal in steady state at a large scale. In some cases a cooling in between discharges by attachment of the armor to cooled backing plates is made. Tore Supra has an actively cooled First Wall and modular limiters designed for steady state heat removal. Actively cooled divertor plates have also been designed for the future use in JET. Experience with these components in Tore Supra suggests that, under real conditions of a fusion device, the reliably handled average heat load is of the order of a few MWm^{-2}, significantly less than the maximum heat removal capability realized with single test components, which is of the order of 20-30 Mwm^{-2}. The design reference value for the average heat load to the divertor in ITER has been presently set to be 5 MWm^{-2}. For comparison, the average wall loading in large conventional thermal power plants using fossil fuels is of the order of 0.3 MWm^{-2}.

To remain within the limit of 5 MWm^{-2}, ITER already requires a divertor with large effective area for heat removal, typically a factor of 10 larger than that of the separatrix strike zones on appropriately designed divertor target plates. The present ITER reference design is based on a deep high density divertor in which charge exchange reactions provide energy and momentum transport to the large area sidewalls. The physics of the concept and the consistency with other boundary conditions is not yet verified. Radiation of a large fraction of the power within the divertor or preferentially within the boundary region of the confined plasma will probably also be required in ITER.

The safety margin for ignition of a reactor increases with the total fusion power produced. The latter is finally limited by the power handling capability of the high heat flux components. Reliably operating components, capable of heat loads well in excess of 5 MWm^{-2}, would be highly desirable already for ITER and will be vital to a safe and economic power reactor and to DEMO.

The erosion of wall material is another challenging problem. In the earlier stages of the ITER project primary sputter erosion rates at the strike point of

up to 10 m carbon per burn year carbon were estimated, neglecting redeposition (the same order of magnitude would apply for beryllium or other low-Z materials). Depending on the degree of redeposition, the net erosion may be reduced by a factor of about 100. The understanding and modeling of erosion and redeposition is still in its infancy. It appears that active methods like in situ film deposition by e.g. gas puffing during the discharge or in situ plasma spraying during plasma pauses will be required. Whether high Z materials are an option for ITER still has to be demonstrated. Operation of ALCATOR C Mod with an all molybdenum wall, experiments on molybdenum and tungsten limiters in TEXTOR and experiments in ASDEX Upgrade may help to provide the necessary data.

Due to the high power, large duty cycles, and due to the large neutron fluences in DEMO and in a power reactor it appears to be very unlikely that any of the materials presently discussed for ITER offer a solution to the erosion problem. New concepts will have to be developed.

One way to solve the above problems may be the use of fluid targets, i.e. moving liquids or solids through the high heat flux zones. The heat is essentially stored in the heat capacity of the matter and transported with the material itself to areas of the device where it can be more easily removed during appropriately long transit times. The cooled down materials would then be recirculated through the high heat flux zone.

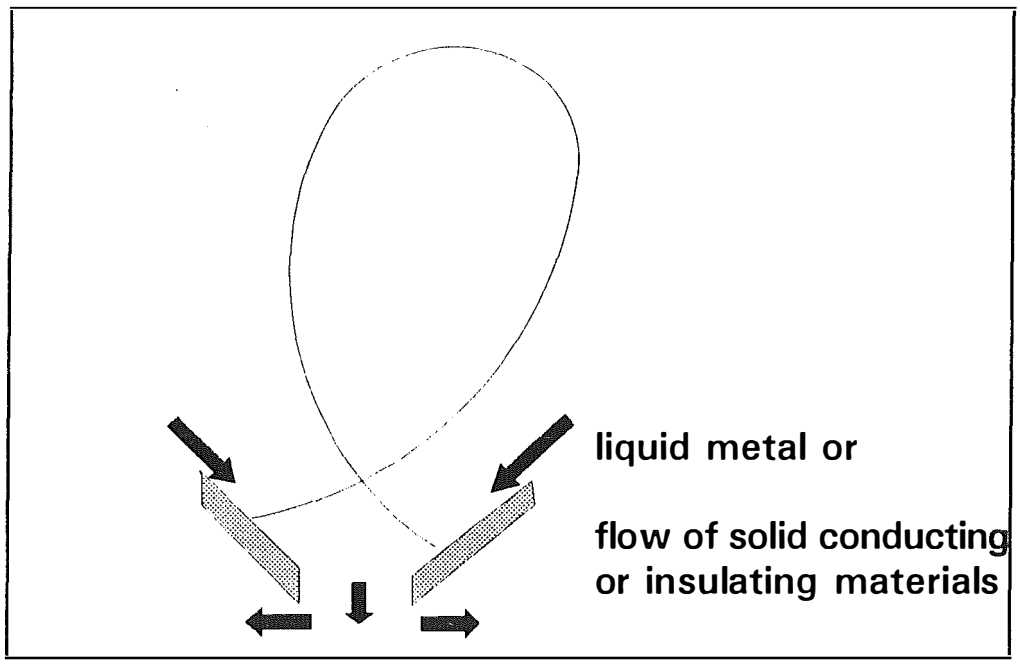

Fig. 1: Fluid target concept: utilize heat capacity by a flow of matter through the high heat flux area

Such a concept would fulfil the requirements for steady state operation by definition and could also solve the erosion problem by replacement of damaged solids or simple readjustment of the surface in the case of liquids. The heat removal capability can be very high (see below). Problems due to radiation damage could be mitigated by the liquid state and/or high temperatures used. New possibilities of particle removal by implantation into the material could possibly be employed.

The large variety of possible fluid target concepts has been structured according to the breakdown scheme shown below. Some of the properties and problems mentioned in the diagram in italic script are discussed in more depth in the following contributions.

fluid targets

liquids (sheets, pools, droplets)		solids (spheres)	
non conducting	conducting	non conducting	conducting
oils	metals	SiC, B_4C	metals

hybrid systems: rotating targets

.....m a i n...c o n c e r n s.....

low heat cond., low ΔT	jXB, MHD instability	fatigue stress	jXB? fatigue?

number of spheres
transport of spheres
heat extraction

Two main classes are distinguished, namely liquids and solids which are again broken down into electrically conducting and non conducting ones. This has turned out to be useful since major problems are the forces induced by the interaction between the magnetic fields in a fusion device and currents induced in a moving conducting medium, and instabilities in the liquid. In the case of metallic liquids the use of droplets may be interesting since their small size limits the current effects but some advantages of a liquid are still retained. No well suited non conducting liquid has been identified, unfortunately. For the non (or badly) electrically conducting solids high temperature materials like graphite, boroncarbide or siliconcarbide appear to be interesting because a high operation temperature could be used. Their plasma-surface-interaction properties are rather well known. A major problem appears to be the thermal stress and fatigue, which could be less pronounced with the more ductile conducting metals. He pumping by implantation could be an option for all solids used. Of concern may also be the large number of elements required for a "solid ball" arrangement. The hybrid group of rotating targets, eventually cooled by liquid metals from the inside, shows some promising properties.

Reference values for the power loading

For the assessments made below a reference value of the power loading of 50 MWm^{-2} has been chosen.

This order of magnitude has been delineated from an ITER type reactor assuming a thermonuclear power generation of 1 GW, of which 20% α power, i.e. 200 MW have to be handled by the divertor, if no significant radiation of power is assumed. With a major radius of 7 m and an effective width of the strike zone on inclined plates of 5 cm on both the inboard and outboard side, the total affected area of the target plate is about 44 m^2 leading to an average heat load of 45 MWm^{-2}.
The value of 50 MWm^{-2} is one order of magnitude larger than that adopted for the present ITER divertor design.

2. Liquid metal targets (J. Winter)

2.1 Possible configurations

A variety of different possible geometries have been proposed in the literature. Among these are:

- protective films (fig. 1),
- pool (fig. 2),
- droplet beam (fig. 3),
- droplet curtain (fig. 4).

Main problems associated with liquid metal targets are:

- contamination of the main plasma by sputtering, evaporation
- heat transfer and pumping requirements,
- MHD stability and equilibrium,
- particle removal and tritium inventory,
- material compatibility,
- transient electromagnetic phenomena, disruptions.

A feasibility study /1/ came to the conclusion, that the most promising concept is that of a curtain divertor using gallium. Lithium metal is unsuited because of the large tritium inventory (hydride formation). The beam concept, in addition to using lithium, seems to create problems of splashing at the beam dump. The slowly moving film and pool solutions are regarded unfavorable with respect to blistering.

table 1, from ref. /1/

Comparison of Different Steady State Divertor Concepts

	Solid	Lithium		Gallium		
	Solid Plate	Li drplt beam	Li Thin Film	Ga Pool	Ga Film	Ga Drplt Curtain
Sputtering erosion	yes	no	no	no	no	no
Insufficient heat removal	no	no	no	no	no	no
Design conflict in erosion and heat transfer	yes	no	no	no	no	no
H embrittlement and exfoliation	yes	yes*	yes	no	no	no
Tritium inventory concern	no	yes*	no	no	no	no
Blistering erosion	yes	yes*	yes	yes	no**	no
Detrimental MHD effects	no	no	no	no	yes	no
Detrimental disruption effects	yes	no	maybe	no	no	no
Limited to lower divertor	no	maybe+	yes	yes	yes	no

* Assuming the efficient Li renewal technology is not available
** Assuming it is a short film divertor (0.1 *m* long) flowing at 10 m/s
\+ Depending on the availability of tokamak space

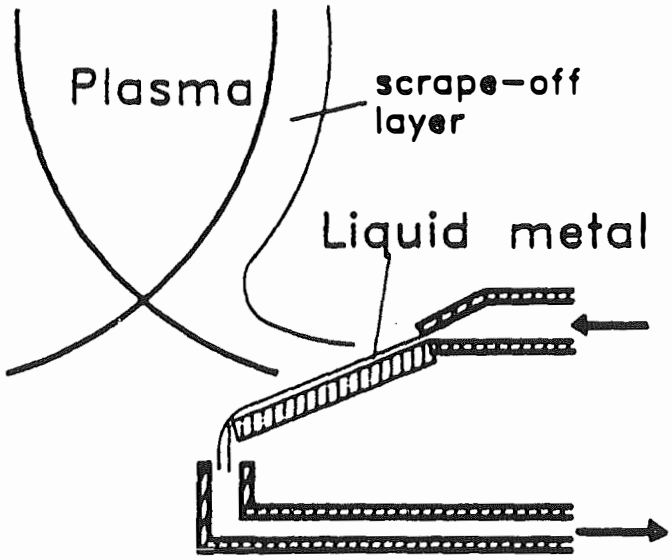

Figure 1: Liquid metal protective film divertor

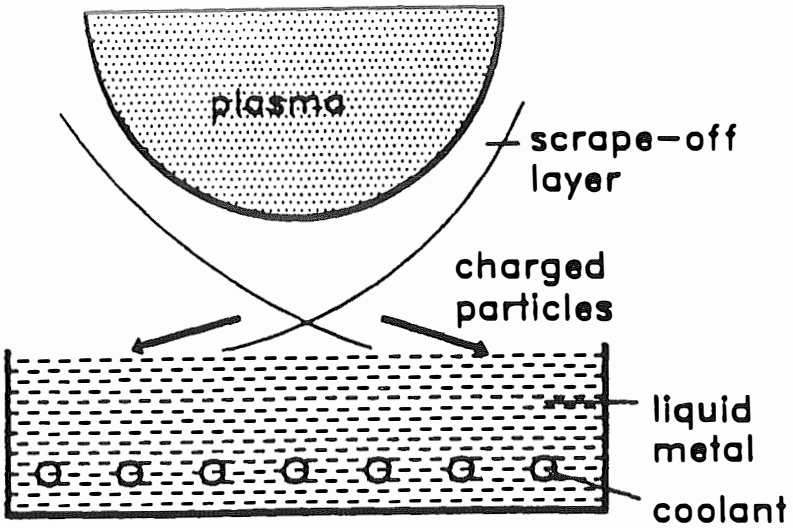

Figure 2: Liquid metal pool type divertor

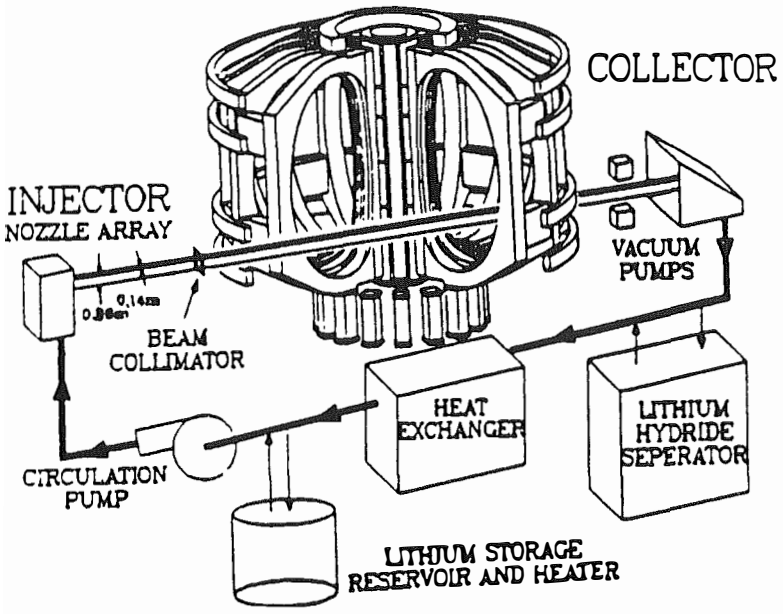

Figure 3: Liquid lithium droplet beam divertor [Werley, 1989]

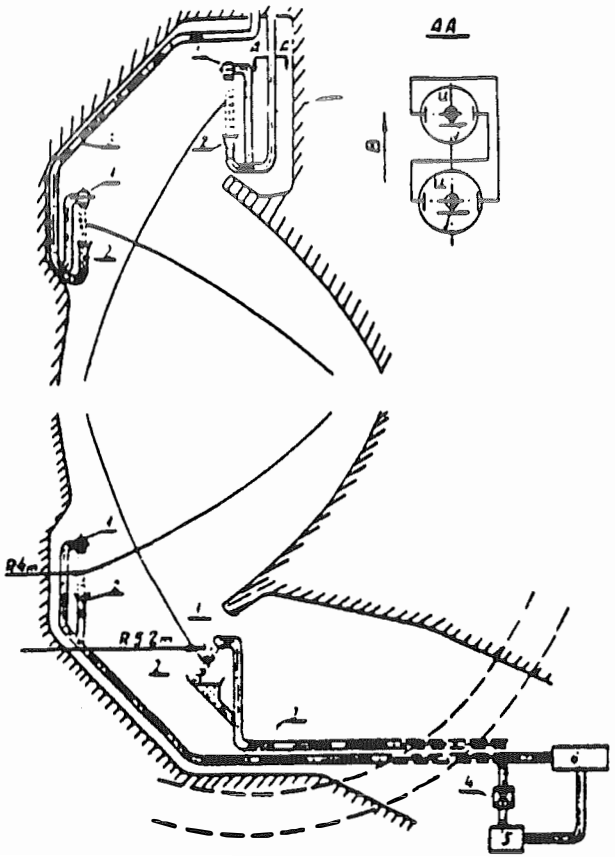

Figure 4: Liquid gallium droplet curtain divertor [Murav'ev, 1989]

The anaylysis presented in this report came to a different conclusion in the sense that MHD effects do indeed pose serious questions on the feasibility of both the pool and film concepts. On the other hand, plasma surface interaction studies over the last decade have shown that blistering is not a major problem, neither in solid nor in liquid materials (see 9. Conclusions).

The two concepts tested experimentally in a tokamak /2/ are those of the protective films and droplet curtain using a gallium eutectic. The results are not conclusive, unfortunately. A sheet limiter failed in a catastrophic mode because of burn out and overheating of the gallium. The flow of gallium was obstructed due to the pulsed operation of B (plasma pulse length typically 50-70 ms) and overheating of the edges occurred. Prior to the overheating the systems seemed to work satisfactory. Splashing of Ga all over the machine occurred. The technical feasibility of a gallium droplet curtain was demonstrated, including the droplet formation and operation of tokamak discharges with the droplet curtain 3 cm inside the scrape-off-layer. A comparison with discharges limited by graphite tiles were made indicating stable operation with some enhanced radiation in the case of Ga during the current rise phase.

2.2 Criteria for selecting liquid metals

A number of criteria apply to the selection of metals for a liquid divertor. Among these are

- reasonably low melting point and low vapour pressure at high temperatures, yielding a large effective temperature range,
- no hydride formation or decomposition of the hydride below the operation temperature,
- good oxygen getter for optimum conditioning,
- compatibility with structural materials.

A number of interesting candidates exist and have been discussed more or less extensively in the literature. Among these are lithium (forms however hydrides which are stable well above the melting point of the metal), gallium, tin and some eutectics of these materials. Another candidate may be aluminum which, despite its poor compatibility in liquid state with most metals, offers the advantage of reasonably low Z (Z=13), technically accessible melting point of 600°C and acceptable vapour pressure up to 1000°C. Beyond that it has a very high affinity to oxygen and the oxide is refractory.

In addition to sputtering the formation of gas bubbles by implanted protons

leading to bursts of metals, and blistering and exfoliation have been mentioned in the literature as possible contamination mechanisms in steady state. Results of implantation studies in solids have shown that the latter mechanisms do only occur under special conditions and that they don not have to be regarded as serious problems. Thus they are not discussed in this report.

Because of the lack of data the sputter yields are assumed to be the same as for the solid state. It has to be considered that the release of material into the plasma is very strongly dependent on actual geometry and whether the liquid metal is used in a limiter or divertor configuration.

At this stage of the study no optimized selection of a liquid metal has been made since more general questions of liquid metal targets are discussed. In order to obtain some quantitative numbers, however, the example of Al has been used in most cases.

2.3 Liquid aluminum

Atomic data

	Aluminum
Z	13
m(molar weight)	26.98
ρ(g/cm13)	2.702
Tm(°C)	660.37
Tb(°C)	2467
heat of evap.(kJ/mol)	293.7
heat of melt.(kJ/mol)	10.67
cv (liquid) (J/molK)	29.3

Aluminum provides a wide temperature span of 1800 °C between the melting and boiling point. It may be expected that it is relatively tolerant to significant heat transients as e.g. during ELMs etc. It also has a large heat of evaporation. One disruption of a high performance discharge in TEXTOR would lead to an evaporation of about 4 g of Al (energy quench only).
Na and K have boiling points of 759°C and 882 °C, respectively and are not suited due to their high vapour pressures at elevated temperature.

Aluminum is not regarded as a toxic material, it is readily available. Al may burn at very high temperatures in an oxidizing atmosphere. Evaporation of the oxide layer seems to be necessary for burning. It is definitively less hazardous in this respect than Li, Na, K.
Gallium (Z = 31, T_m = 29.8 °C, T_b = 2403 °C) is probably toxic and has a high value of Z. It has very favourable other properties, in particular low melting point and low vapour pressures at high temperature.

A list of the binary alloys of aluminum is given in table 2.

table 2: Liquid binary alloys M-M'(liquidus temperature T_l and vapor pressure of M' at 1000 °C) (from K. Hilpert)

alloy	composition	T_l (°C)	p(M') at **1000 °C** (mbar)
Al-Ga	70 at% Ga	300	2×10^{-3}
Al-Mg	50 at% Mg	460	300
Al-Zn	50 at% Zn	520	1000
	90 at% Zn	400	
Al-Cu	17 at% Cu	550	5×10^{-5}
Al-Ni	T_l strongly increasing		10^{-7}
	10 at % Ni	800	
	2.7 at % Ni	630	
Al-Co	T_l strongly increasing		10^{-7}
	10 at% Co	950	
Al-Fe	T_l strongly increasing		3×10^{-7}
	10 at% Fe	1000	

Al-Mn	T_l strongly increasing 10 at% Mn	870	$3x10^{-2}$
Al-Cr	T_l strongly increasing 10 at% Cr	980	10^{-6}
Al-V	T_l strongly increasing 10 at% V	1200	10^{-10}

Oxygen gettering

Aluminum has a very strongly bound oxide Al_2O_3 with high melting point and low vapour pressure (T_m = 2072 °C, T_b = 2980 °C). The bond energy per oxygen atom can be regarded as figure of merit for the O-getter potential. Al is expected to be an even better oxygen getter than B and Si and comes close to Be, which all have proven their efficiency in tokamaks (TEXTOR, JET).

table 3: Free energy of formation ΔG and free energy of formation per oxygen atom ΔG/O for various oxides (25 °C)

Z	atom	oxide	-ΔG[kJ/mol]	-ΔG/O[kJ/mol]
4	Be	BeO	581	581
5	B	B_2O_3	1194	397
12	Mg	MgO	569	569
13	Al	Al_2O_3	1582	527
14	Si	SiO_2	857	428
22	Ti	TiO_2	889	444
73	Ta	Ta_2O_5	1911	382
24	Cr	Cr_2O_3	1058	352

Vapour pressure and evaporation rates

The vapour pressure at the melting point is about $5x10^{-9}$ mbar, that at 1000°C is about $2X10^{-4}$ mbar. It is less than that of Ga over the whole temperature range.

The evaporation rate at the melting point is about $1X10^{16}$ $m^{-2}s^{-1}$, and is $5X10^{20}$ $m^{-2}s^{-1}$ at 1000°C. A surface of 4 m^2, as an example, yields a total evaporation rate of 2×10^{21} s^{-1} at 1000°C. This corresponds to about 2 monolayers per second on the entire first wall of the TEXTOR device. At the melting point of 660°C these values are smaller by a factor of $5X10^4$.

The sputter flux (only D-sputtering) at a yield of 0.03 (500 eV) and at a total D-flux of about 10^{21} s^{-1} is $3X\ 10^{19}$ s^{-1}.

Thus, between the melting point and 1000 °C the evaporation rate changes between negligible compared to sputtering and about 60 x the sputter rate. This behaviour may be used to advantage for controlling the seeding of the SOL with Al for establishing a radiative boundary. It has to be kept in mind, that thermal evaporated Al atoms will have a very short penetration depth only and that a large fraction will be locally redeposited (depending also on the actual geometry chosen).

Heat removal

The heat conductivity is

λ[W/mK]	238	115	121
T[°C]	20	700	790

the specific heat is

C_p[J/g K]	1.14	1.04
T[°C]	650 (s)	660 (l)

Assuming heat conduction only and a tolerable temperature increase ΔT = 400 °C, i.e. 1060 °C at the surface and 660 °C at the cooled side, the allowed thickness to accommodate $50MW/m^2$ heat load is about 1 mm liquid Al.

Since λ is larger in the solid phase, this may lead to solid Al at the cooling structures when the system is designed to be at 1060 °C at the surface. It may be speculated whether this can be used to provide a solid Al reservoir for further melting in case of heat transients.

Natural convection in form of vertical vortices may occur in a pool design due to temperature gradients between surface and bottom. Heat would be dispersed over a larger volume.

If mass flow of Al is considered, the specific heat can accommodate 1.04 J/g K in the liquid phase. Assuming a temperature increase of 400 °C the accommodated energy is 416 J/g.

In order to remove the total of 200 MW in ITER a circulation of about 0.5 tons of liquid Al, i.e 0.18 m^3s^{-1} is required, assuming homogeneous heating.

Assuming a flowing film with a thickness of 0.5 cm and homogeneous heating, the handling of 50 MWm^{-2} requires a flow velocity of about 9 ms^{-1} at $\Delta T = 400°C$.

Viscosity

The dynamic viscosity decreases somewhat with increasing temperature. Already at 662 °C it is close to that of water at 20°C.

η [$mNsm^{-2}$]	1.38	1.28	1.102
T [°C]	662	700	800

(water :1 $mNsm^{-2}$)

Flow in the presence of a magnetic field is influenced: motion parallel to B is essentially unhindered whereas friction forces occur for motion perpendicular to B.

Electrical resistivity

(from Landolt-Börnstein)

The electrical resistivity increases at the melting point and with increasing temperature.

ρ [$\Omega mm^2/m$]	0.028	0.287	0.293	0.308	0.337
T [°C]	20	700	800	900	1000

It is at 700 °C about 160 times larger than that of Cu at 20°C and is of the same order as that of Inconel at 20°C.
It may be possible to heat Al by passing a direct current through it.

References

/1/ C. Liao and M.S. Kazimi, Fusion Technology 21,1845 (1992)

/2/ S.V. Mirnov, V.N. Dem'yananko and E.V. Murav'ev, J.Nucl. Materials 196-198, 45 (1992)

3. Electromagnetic fields and forces on a liquid metal limiter (A. Kaleck)

Introduction:

In a tokamak metal structures are exposed transient electromagnetic fields. The larger the structures the more dangerous are the forces on them. Solid structures can be stabilized by mechanical supports. Liquid metal films which are considered to be used for the heat transport in a limiter or divertor not only experience additional forces by the motion of the metal but also are kept at their base only by gravity. Therefore the forces on this films caused by time- and space-varying electromagnetic fields have to be considered carefully.

In a USSR contribution to the INTOR Workshop 1987 in Vienna a group of the Efremov Institute [1] only considered the EMF $\underline{v} \times \underline{B}_{Pol}$. In this paper we try to estimate the consequences of the relevant forces on liquid metal films caused by time- and space-varying electromagnetic fields, e.g. disruptions and inhomogeneous poloidal and toroidal fields. Also a rough estimate was made for the Rayleigh-Taylor surface instability.

I. Schematic View, Geometry and Exemplary Configuration

Fig. 1 shows a poloidal cut of a possible limiter configuration. The liquid metal streams from an upper reservoir along an oblique plane into a lower reservoir touching the outer magnetic surfaces of the plasma.

In Fig. 2 the liquid film is turned by the angle φ into the horizontal plane to explain the coordinates used later. The metal is to flow in the negative x-direction, the toroidal-magnetic field is in the y-direction and the poloidal field is in the x-z plane.

---

[1] "Impurity Control, First Wall, Blanket"
USSR Contribution to INTOR Workshop Phase IIA, Part 3, Session XV, Vienna July 13-24, 1987

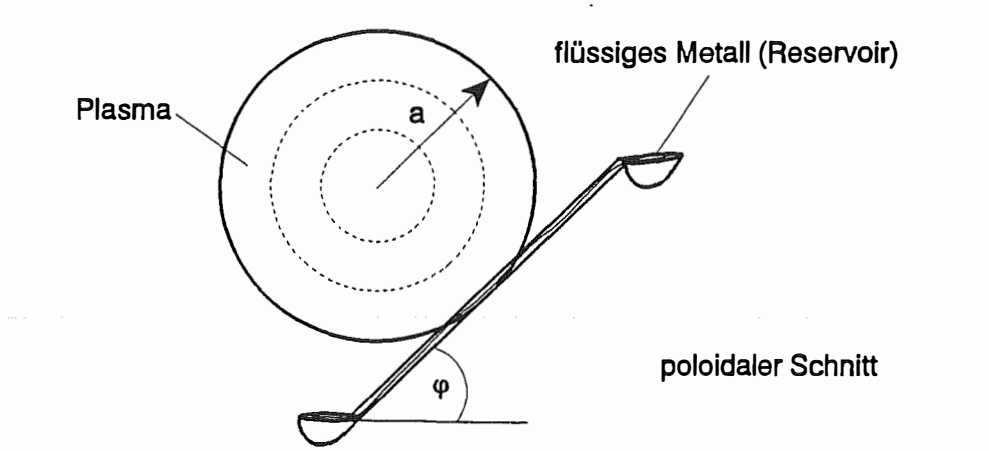

Fig. 1 Schematic view of a liquid metal limiter - poloidal cut

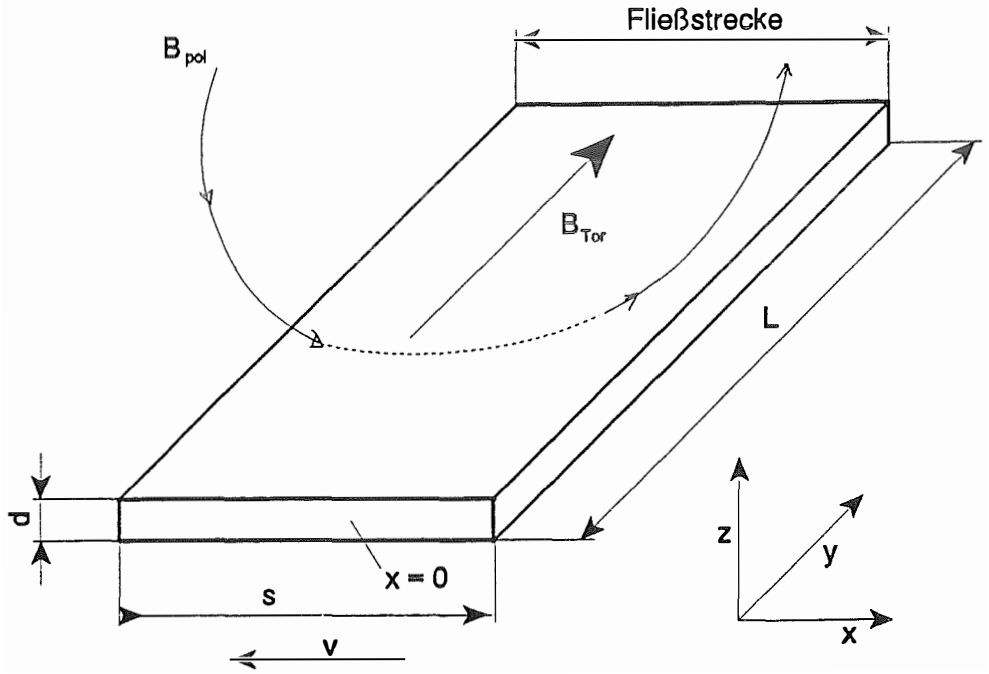

Fig. 2 Geometry and coordinates of liquid metal film

As an example for an experiment a TEXTOR limiter-configuration is specified.

<u>TEXTOR dimensions</u>	
large radius	$R_0 = 1.75$ m
small radius	$a = 0.5$ m
toroidal field	$B_{Tor}(R) = R_0/R \cdot 3\ T_s$
poloidal field	$B_{Pol} = 0.2\ T_s$
<u>liquid Al</u>	
electric resistivity	$\rho_{el} = 3 \cdot 10^{-7}\ \Omega/m$
specific weight	$\rho = 2.7 \cdot 10^3\ kg/m^3$
viscosity	$\eta = 10^{-3}\ NS/m^2$
<u>moving liquid metal film</u>	
angle	$\varphi = 45°$
streaming distance	$s = 0.5$ m
toroidal segments	$L = 1$ m
thickness	$d = 0.5$ cm
velocity	$v \approx 1$m/s

II. Induced currents and forces during a disruption

During a disruption of e.g. TEXTOR a loop voltage of about 100 V can be expected. If the liquid limiter is axisymmetric a loop current around the torus will be induced with a current density

$$j = \frac{100 Volt}{2\pi R_0 \cdot \rho_{el}} = 30 MA/m^2$$

which corresponds to a total current of 75 KA in the same direction as the plasma current. So the metal film will be attracted by the plasma current with a force density

$$k = j \cdot B_{Pol} \approx 6 \cdot 10^6 N/m^3$$

while the gravitational force is only

$$\rho \cdot g \cdot \sin\varphi \approx 1.9 \cdot 10^4 N/m^3 \ .$$

This causes an acceleration of the liquid metal of

$$b = 2000\ m/s^2$$

which will lift the liquid a few centimeters during the disruption.

To avoid this, the axisymmetric metal film has to be toroidally segmented into segments of length "L".

By the decay of the vertical field

$$\frac{d}{dt} B_{vert} \approx \frac{0.1\,T_s}{15\,ms}$$

a loop current on the metal film in the x-y plane will be induced (Fig. 3) which can be estimated as

$$j \approx \frac{E}{\rho_{el}} \ ; \quad E = \frac{\dot{B}_{vert} \cdot F \cdot \cos\varphi}{2(S+L)} = \frac{\dot{B}_{vert} \cdot S \cdot L \cdot \cos\varphi}{2(S+L)}$$

$$j \approx 2.6 \cdot 10^6\ A/m^2 \ .$$

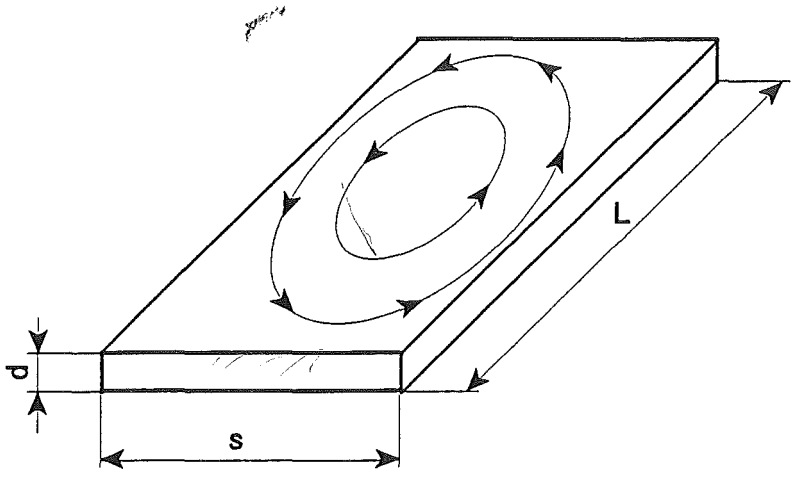

Fig. 3 Current loop induced by the decay of vertical magnetic field

to calculate

The x-component of this loop current leads with B_{Tor} to a force perpendicular to the x-y plane in opposite directions for y ≈ 0 and y ≈ L. The force density is

$$k = j \cdot B_{Tor} \approx \frac{\dot{B}_{vert} \cdot S \cdot L \cdot B_{Tor} \cdot \cos\varphi}{2(S+L) \cdot \rho_{el}} \approx 1.6 \cdot 10^7 \; N/m^3$$

which is even larger than the force by the toroidal loop current.

This force can be reduced to a tolerable value, by segmenting the metal flow in the toroidal direction into "filaments" of 1 cm width which had to be electrically isolated against each other.

Since this seems not to be practicable by constructional reasons the liquid metal of a limiter/divertor will be shot into the vacuum chamber during a disruption.

III. Stationary Flow

1. Fluid flow and viscosity

We look at the metal liquid as an incompressible fluid. We neglect the deviation of the flow lines in z-direction, that is

$$\underline{v} = v_x \cdot \underline{e}_x$$

and $$v_x \cdot d(x) = constant$$

with d(x) the thickness of the liquid film. A gravity driven fluid on an inclined plane (φ) will be accelerated to the velocity

$$v(x) = -[2g \sin\varphi \left(\frac{s}{2} - x\right)]^{1/2}$$

(with $\rho \dot{v} = -\rho g \sin\varphi$ *and* $\frac{\partial}{\partial t} = v \frac{\partial}{\partial x}$).

Fig. 4 shows $v_x(x)$ and d(x) for the examplary experiment. Viscosity will not play any role since the friction force

$$\eta \frac{\partial^2 v}{\partial z^2} \approx \eta \frac{v}{d^2}$$

is small compared to the gravitational force $\rho \cdot g \cdot \sin \varphi$ at the considered velocity.

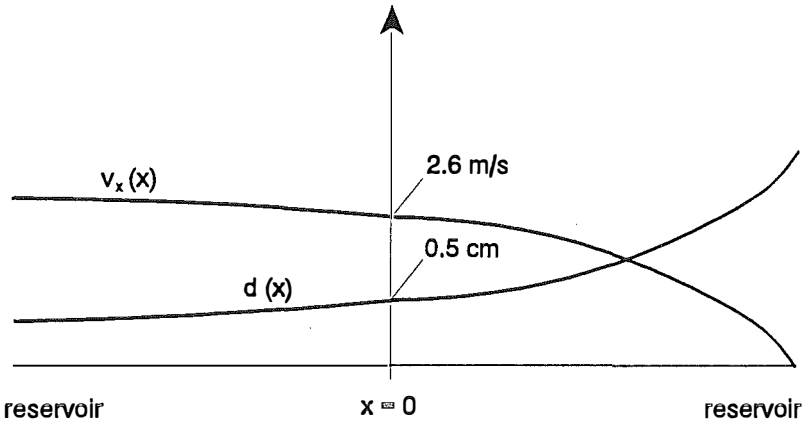

Fig. 4 Flow velocity and thickness of the liquid metal film under gravitational force

2. Field penetration

A moving fluid element will see remarkable field fluctuations at a time scale of

$$\tau > 10 ms \ .$$

The penetration depth will be

$$\Delta_{skin} = \left(\frac{\rho_{el} \cdot \tau}{\mu_0} \right)^{1/2} \approx 10 cm > d \ .$$

The induced currents can therefore be treated as volume currents.

3. Currents induced by the fluid motion

The electric field

$$E_y = v_x \cdot B_z$$

induced by a B-component vertical to the fluid plane was considered in [1] and it was proposed to segment the limiter in the toroidal direction and to apply an additional electric

field to avoid the induced y-current. Here we consider current loops induced in the conducting fluid by the motion into a region of increasing $B_{Tor} \sim 1/R$ and also cuts the magnetic surfaces.

a) Effect of inhomogeneous B_{Tor}

A fluid element $d \cdot L \cdot dx$ moving with velocity v in an inhomogeneous B_{Tor}-field experience an induction in the x-y plane

$$\dot{\Phi} = d \cdot dx \cdot |v| \frac{d}{dx} B_{Tor} = d \cdot dx \cdot |v| \frac{B_{Tor}}{R_0} \cdot \cos\varphi$$

and "elementary" current loops are induced

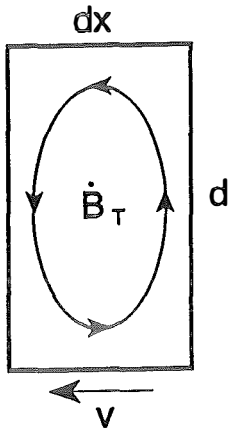

Fig. 5 Elementary current loop

The j_z-components almost cancel out and we will essentially get one current loop, the exact location of which is determined by the boundary conditions at the reservoir (Fig. 6).

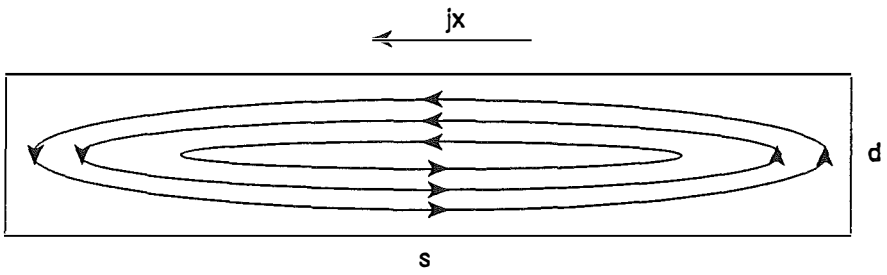

Fig. 6 Current loop induced by the motion of the liquid metal into higher B_{Tor}-field

Since d ≪ s it follows

$$j_x \gg j_z \quad [1]$$

and we can write

$$\dot{\Phi} = -\int Eds \approx 2 \cdot dx \cdot j_x \cdot \rho_{el}$$

and

$$j_x \approx \mp \frac{v B_{Tor} \cdot \cos\varphi \cdot d}{2 R_0 \cdot \rho_{el}}$$

with the "-" sign at the upper surface. This current loop tries to keep the B_{Tor} constant inside the fluid. So the outer B_{Tor} acts as a pressure at the fluid surface and may cause a Rayleigh-Taylor instability [2].

Comparison of this magnetic pressure with the restoring force $\rho \cdot g$ results in

$$\frac{p_{Dr}}{p_{rest}} = \frac{v \cdot d \cdot B_{Tor}^2 \cdot \cot\varphi}{2 R_0 \cdot \rho_{el} \rho \cdot g} \approx 300 \gg 1$$

i.e. the metal surface is unstable against the Rayleigh-Taylor instability.

The growth time can roughly be estimated by

$$\tau \approx \left(\frac{Mass}{k_{Driv}} \right)^{1/2} .$$

The accelerated mass is that of the shadowed region in Fig. 7

$$Mass \approx \frac{\rho \cdot \lambda \cdot h}{8} .$$

---

[1] The j_z-component is too small to influence the v_x motion.

[2] J.A. Wesson, "Plasma physics and nuclear fusion research", Academic Press London 1981, Edited by R.D. Gill (p. 191 ff).

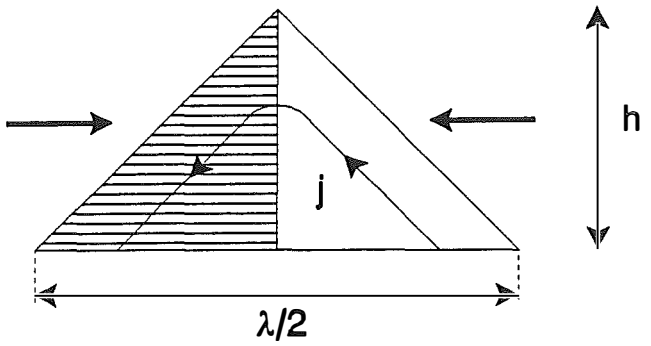

Fig. 7 Surface perturbation of the liquid film, the j_z-component builts with B_{Tor} the driving force of the instability

The driving force is the volume force $j_z \times B_{Tor}$ integrated over the same region

$$k_{Driv} \approx \frac{\nu \cdot d \cdot B_{Tor}^2 \cos\varphi \cdot h}{4 R_0 \rho_{el}}$$

k_{Driv} is the specific driving force K_{Driv}/(amplitude h)

$$\Rightarrow \quad \tau = \left(\frac{\rho \cdot \rho_{el} \cdot \lambda R_0}{2 \cdot \nu \cdot d \cdot B_{Tor}^2 \cos\varphi} \right)^{1/2} \approx 8 \cdot 10^{-3} \sqrt{\lambda} \ [s] \ .$$

For a perturbation $\lambda \approx d$ for the growth time we get

$$\tau \approx 0.5 \ ms \ .$$

This instability should destroy the liquid metal surface. It is avoidable only by a perpendicular arrangement of the metal film ($\cos\varphi = 0$).

b) Effect of touching the magnetic surfaces of the plasma

Generally the limiter is to scrape-off some outer magnetic surfaces of the plasma. This has the consequence that the B-component vertical to the limiter is inhomogeneous. Fig. 8 shows that a moving fluid element will see a vertical B-component which is changing sign. This leads to a further current loop sketched in Fig. 9. In the x-y plane the j_x-component acts

with the toroidal field to give forces at y ≈ 0 and y ≈ L in the z-direction with opposite sign. The force density can easily be estimated in a similar way as before.

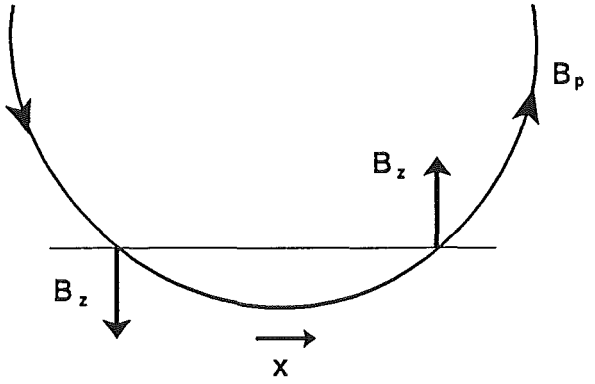

Fig. 8 B_{Pol} cuts the metal surface by moving into the -x direction the fluid first sees a positive and than a negative B_z-field

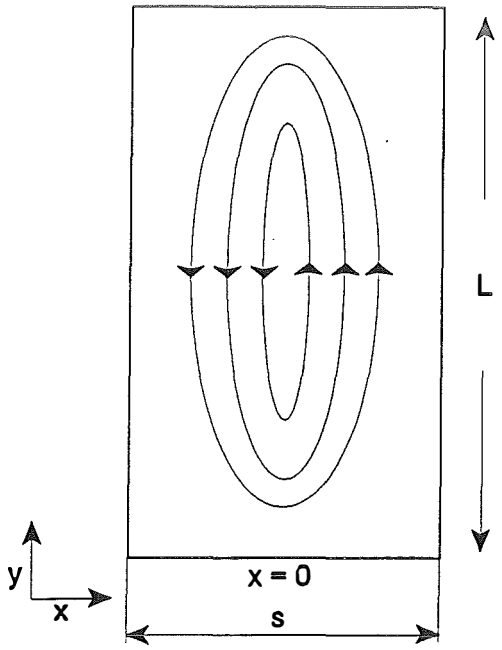

Fig. 9 Current loop in the x-y plane induced by the motion into a changing B_z-field

$$k_z \approx \pm \frac{v \cdot B_{Tor} \cdot B_{Pol} \cdot L \cdot S}{2a\rho_{el}(L+S)} \; N/m^3 \approx \pm 10^6 \; N/m^3$$

(remember the gravitational force density is $k_s = 1.3 \times 10^4$ N/m^3).

This leads to an acceleration of

$$b \approx 370 \; m/s^2$$

and to a shooting of the liquid metal into the plasma chamber.

IV. Conclusions for the liquid metal limiter/divertor

Disruptions of the plasma current causes forces by the decay of the poloidal field which does not allow practicable liquid metal films in the vicinity of the plasma.

In the stationary phase the operation of a liquid metal as a limiter/divertor also seems impossible since the fluid moves into a spatially varying poloidal B-field and the metal will be shot into the plasma chamber.

The Rayleigh-Taylor surface instability will destroy the metal surface when the fluid is moving in a region of varying toroidal magnetic field. Since the mode is highly unstable this could be avoided only with a very nearly perpendicular arrangement of the metal film.

Whereas we don't see a possibility to use a liquid metal film as a limiter/divertor target, it may be worth while to look at a target consisting of metal droplets or rigid spheres. Some considerations about these are described in the appendix.

Appendix: Metallic droplets or rigid spheres as targets

a) Since the problems of a metal film came from the large dimensions of connected electrically conducting structures, the metallic spheres have to be electrically isolated from each other.

b) For spheres of radius a $\leq$ 0.5 cm the deflection by an inhomogeneous magnetic field (diamagnetic force) should be negligible.

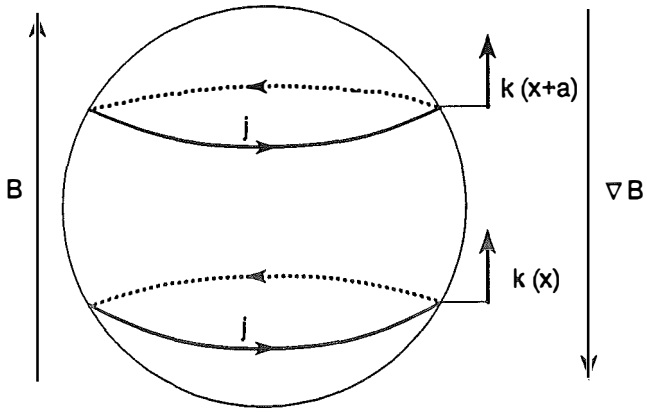

Fig. 10 A net force upward acts on the droplet if there is a gradient in $\underline{B}$

$$\gamma = \frac{k(x+a) - k(x)}{\rho g} \approx \frac{B \cdot \frac{dB}{dx} \cdot a^2 v}{\rho_{el} \cdot \rho \cdot g} \leq 500 \cdot a^2 \approx 10^{-2} \text{ for } a = 0.5cm$$

γ is the ratio of the diamagnetic to the gravitational force.

c) Liquid metal droplets moving into an increasing magnetic field will be compressed to an ellipsoids with the long axis in the direction of the magnetic field.

The compressing pressure can be estimated as

$$p_m = \beta \frac{vB\frac{dB}{dx} \cdot a^2}{3\rho_{el}}$$

$\beta < 1$ is a numerical factor.

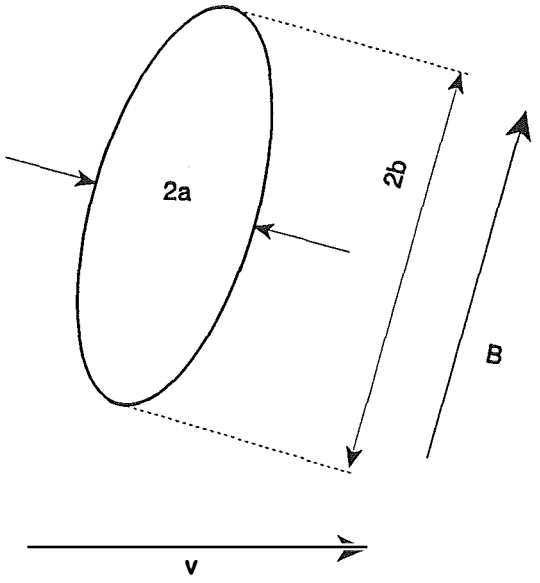

Fig. 11 *The droplet will be compressed to an ellipsoid by the motion into an inhomogeneous perpendicular magnetic field (B_{Tor})*

The restoring force which tries to form an ideal sphere is the surface tension which produces a pressure

$$p_s = \frac{\alpha}{a}$$

with α the surface tension constant $\alpha_{Al} = 0.86$ N/m. The ellipsoid is in equilibrium if

$$p_m = p_s \ .$$

With the radius "o" of the original droplet we get with $o^3 = a^2b$ (constance of volume) and

$$f = \frac{\beta v \cdot B \cdot \frac{dB}{dx} \cdot o^3}{3 \rho_{el} \cdot \alpha}$$

where $f = \frac{b}{a}$.

For too large values of f the droplets may sputter uncontrollable into smaller particles which should be avoided. Therefore f must be smaller than $f_0 \approx 2$ and we get for the radius of the

liquid droplets the condition:

$$o < \left(\frac{3\rho_{el}\alpha \cdot f_0}{\beta \nu B \frac{dB}{dx}} \right)^{1/3}$$

with $\beta \approx 1/4$

$\alpha = 0.86$ N/m

$o \leq 0.6$ cm

Droplets with a radius less than 0.6 cm should satisfactorily keep their form.

4. Temperature distribution and stresses in spherical particles at high flux loading (G. Breitbach)

In a fusion device the divertor is a component exposed to very high heat fluxes. An optimal concept for heat removing is here one of main goals. Beside classical cooling concepts the use of fluid targets is in discussion. One idea is in this context the heat removal by a moving formation of small balls: the balls roll (or slide) along an inclined plane inside the fusion vessel with a velocity in the range of 1m/s; they are there exposed to heat fluxes as high as 50 MW/qm.
In the analysis a single ball of SiC (diameter 10 mm) is considered under such high heat flux loading conditions. It is conservatively assumed that the ball slides so that the it has always the same orientation with respect to the heat flux direction.
The result is that in 40 milliseconds the top of the sliding ball is heated up to temperatures of more then 1500 Celsius with a steep temperature gradient at the surface. In the balls center at this time temperatures have still the initial values. The calculated thermally induced stresses exceed the strength values of the SiC-material.
The effectivity of the heat removal is not very high. For rolling balls the situation is not analysed, but it seems to be not so dramatic. But a tendency to sliding for balls rolling in a formation is given by the fact that touching particles hinder the rolling motion.

Important aspects with respect to a technical realisation:

-Usage factor of the heat capacity with respect to allowable temperatures
-Stability of the moving ball formations
-Fracture of particles (selection of defect particles)

1. Figure:
A surface area with characteristical dimension L is exposed to a heat flux. For short times an analytical solution can be given. It is possible to define dimensionless quantities and to formulate the equation in a quite general manner.

2. Figure:
Evaluation of the formula given in Fig. 1; it is possible to draw the temperature parameter as a function of the dimensionless position or as a function of the dimensionless time. In the upper diagramm the curve $\xi=0$ gives the surface temperature over time.

3. Figure:
Based on the results of Fig. 1 and 2 the diagram is developed for SiC-material and a characteristic length of 10mm. After 40 milliseconds a temperature of 1500 Celsius is reached at the surface, on the other hand at a depth of 1 mm the temperature is still below 200 Celsius.

4. Figure:
Finite Element Analysis, short task description; the local heat flux depends on the orientation of the surface element with respect to the flux direction. It is assumed that the ball orientation is fixed (sliding ball).

5. Figure
Axisymmetrical FE-mesh of the 10mm-ball; finer discretisation in the upper part which is exposed to the high heat flux.

6. Figure:
Temperature over time for the 4 marked positions. It should be noted that the curve 1 is in a good agreement with the surface curve in Fig. 3 although the geometrical configuration is an other one.

7. Figure:
The temperature distribution along the surface from the top to the equator of the sphere is shown at different times on a ten millisecond-scale.

8. Figure:
The temperature distribution from the top to the center of the sphere for the same time points as in Fig. 7.

9. Figure:
Analysis of the thermal effectivity of a sphere: the maximal possible heat content is given for an allowable temperature. The stored heat in the inhomogeneous heated sphere is much smaller the the theoretical maximum.

10 Figure:
Unloaded and displaced mesh: It is clearly to see that the hot upper part of the ball is expanded but constrained by the cold lower part.

11. Figure:
Principal stresses at time t=10,5 milliseconds for the black region; at this time the surface temperature at the top is 800 Celsius. High compression stresses are found at the surface, inside in the cold part lower but more extended tension stresses are observed.

12. Figure:
Principal stress distribution along the line "top-center" of the ball. The compression stress at the nodal point 1 is as high as 1700 MPa. The tension stress maximum is found a little inside reaching 275 MPa.

13. Figure:
It is demonstrated that a rolling motion is hindered if balls are rolling in a dense formation. The friction forces between a ball and the inclined plane (responsible for the rolling!) are opposite to the friction forces between touching balls.

1. FIGURE

HIGH HEAT FLUX REGION

Short term behaviour for temperature penetration depth $<<$ L

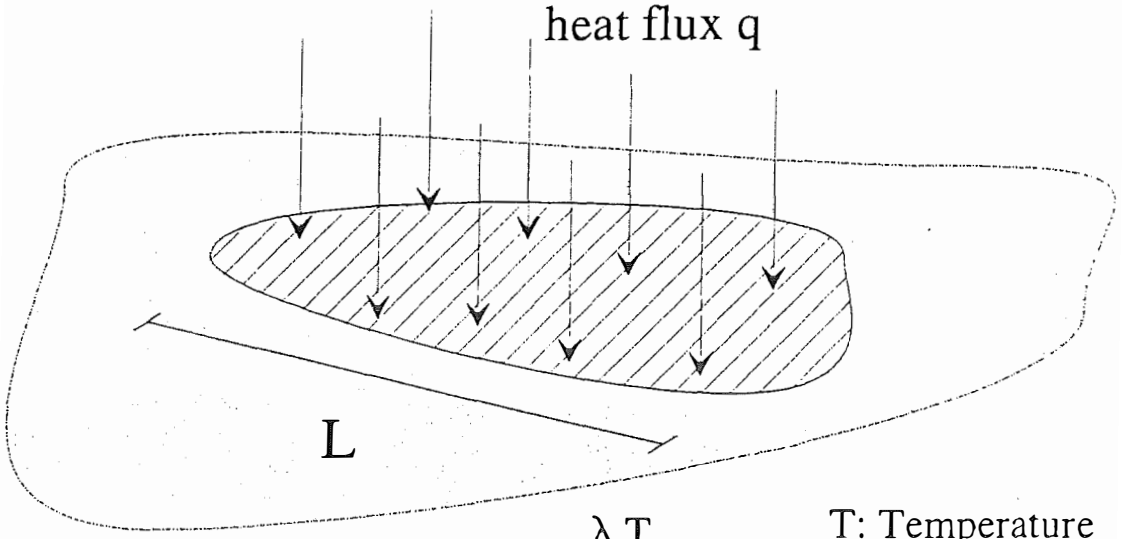

$$\theta = \frac{\lambda T}{q L}$$

$$\xi = x/L$$

$$\tau = \frac{\lambda t}{\rho c L^2}$$

T: Temperature
ρ: Density
λ: Conductivity
x: Distance from surface
c: Spec. heat

Solution of the problem:

$$\Theta(\xi,\tau) = \tau - \xi + \frac{1}{2}\xi^2 + \frac{1}{3} - \frac{2}{\pi^2}\sum_{n=1}^{\infty}\frac{(-1)^n}{n^2}\exp(-\tau\ n^2\pi^2)\cos(n\pi\xi)$$

2. FIGURE

TEMPERATURE-TIME
for given positions

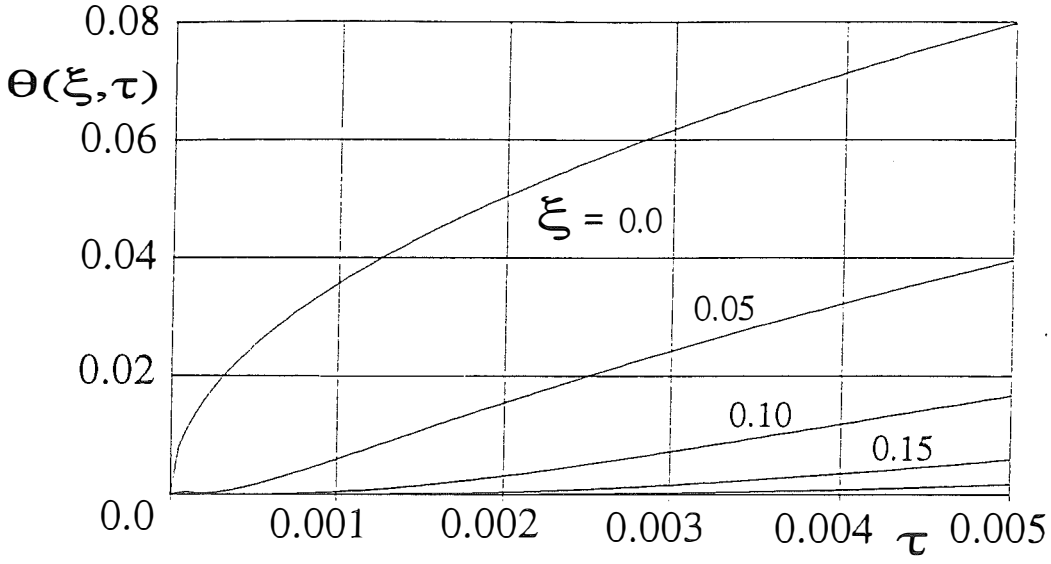

TEMPERATURE-POSITION
for given times

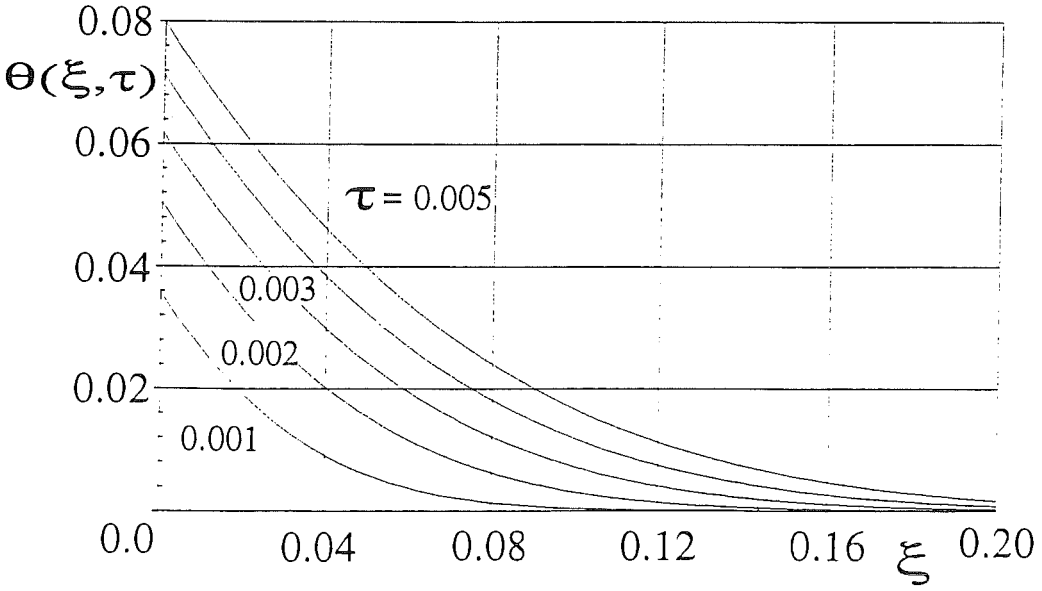

3. FIGURE

AUSWERTUNG FÜR SiC:

$\lambda = 20 \frac{W}{mK}$

$\varrho = 3 \frac{g}{cm^3}$

$c = 1 \frac{J}{gK}$

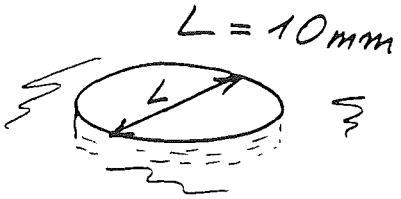

$q = 50 \frac{MW}{m^2}$ (einfallende Wärmestromdichte)

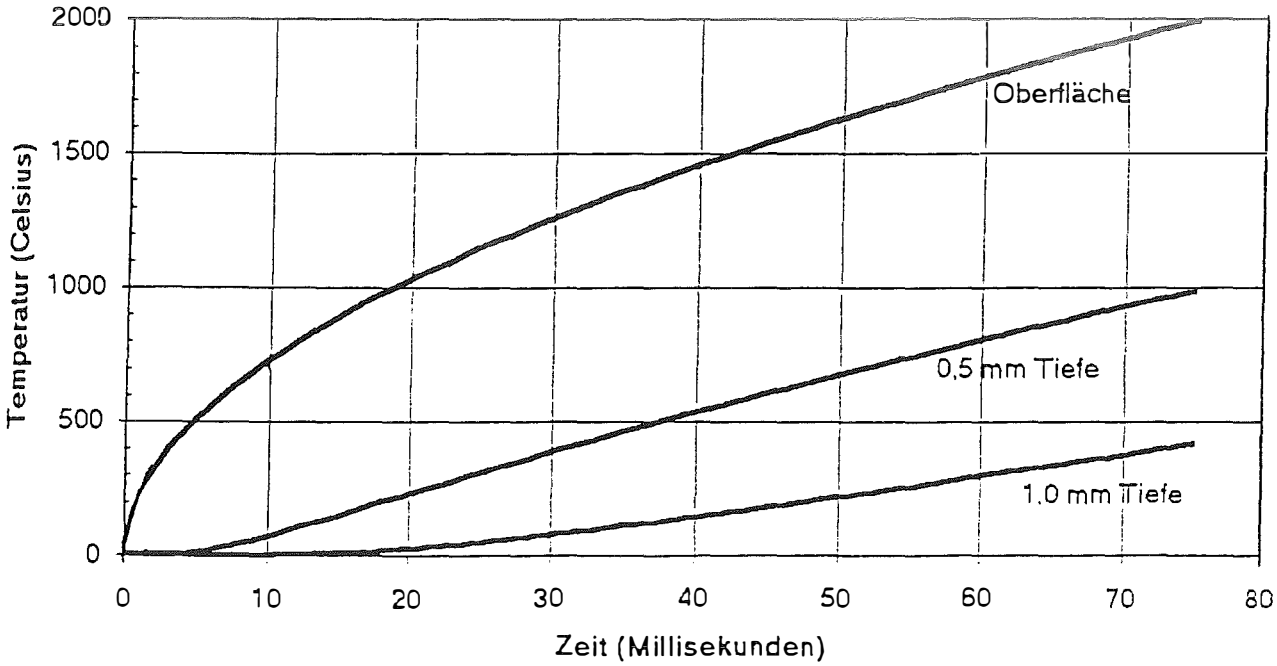

Aufgabentitel: Thermomechanische Analyse einer durch Wärmefluß beaufschlagten Kugel

Problembeschreibung:

(Natur des Problems, Struktur, Belastung, Randbedingungen etc.)

Eine SiC-Kugel erfährt einseitig einen Wärmefluß von 50 MW/qm

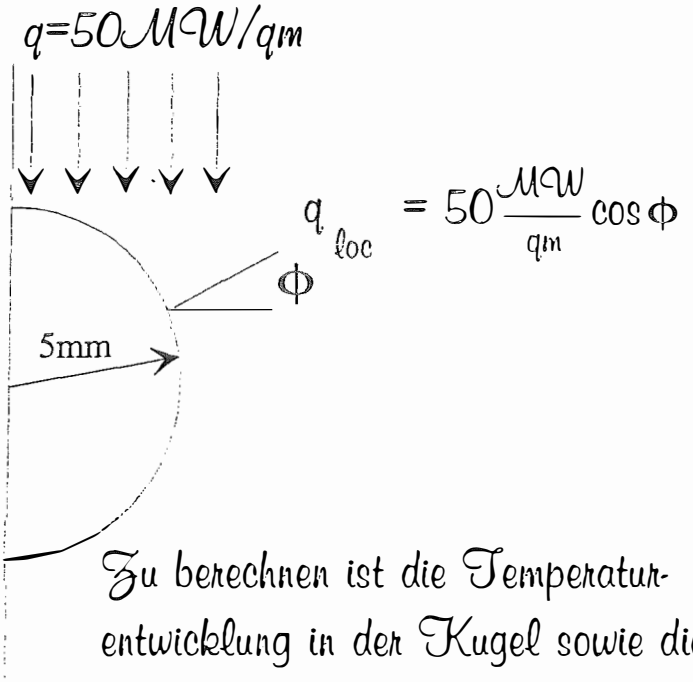

Stoffwerte:

λ= 20 W/mK
ρ= 3 g/ccm
C = 1 J/gK
E = 400 GPa
ν= 0,3
α= 5.0 E-06 1/K

Zu berechnen ist die Temperaturentwicklung in der Kugel sowie die damit verbundenen Thermospannungszustände (elast. Analyse)

5 FIGURE

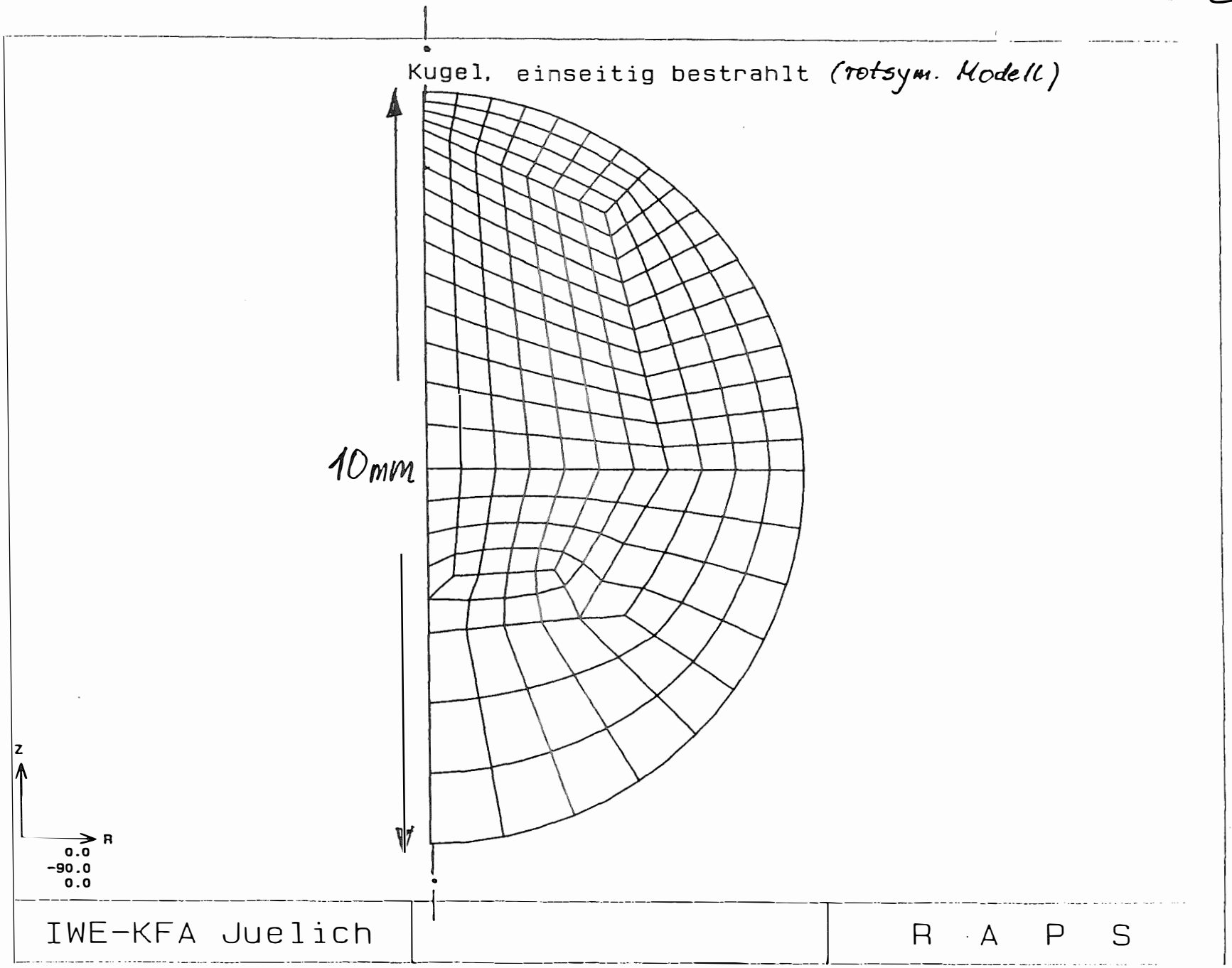
Kugel, einseitig bestrahlt (rotsym. Modell)
10mm
Z
R
0.0
-90.0
0.0
IWE-KFA Juelich
R A P S

6. FIGURE

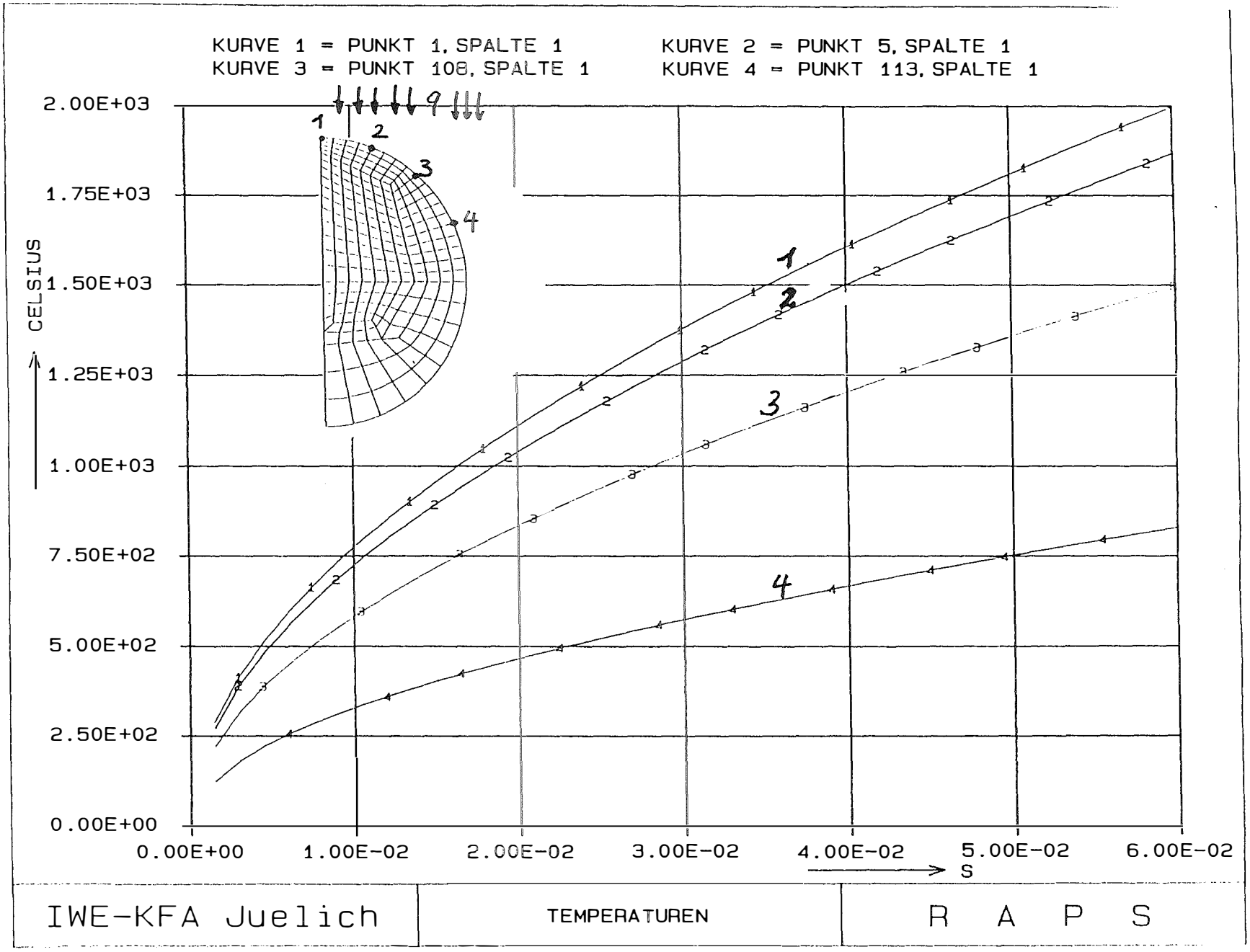
KURVE 1 = PUNKT 1, SPALTE 1
KURVE 2 = PUNKT 5, SPALTE 1
KURVE 3 = PUNKT 108, SPALTE 1
KURVE 4 = PUNKT 113, SPALTE 1
2.00E+03
1.75E+03
1.50E+03
1.25E+03
1.00E+03
7.50E+02
5.00E+02
2.50E+02
0.00E+00
CELSIUS
0.00E+00
1.00E-02
2.00E-02
3.00E-02
4.00E-02
5.00E-02
6.00E-02
S
1
2
3
4
IWE-KFA Juelich
TEMPERATUREN
R A P S

4. FIGURE

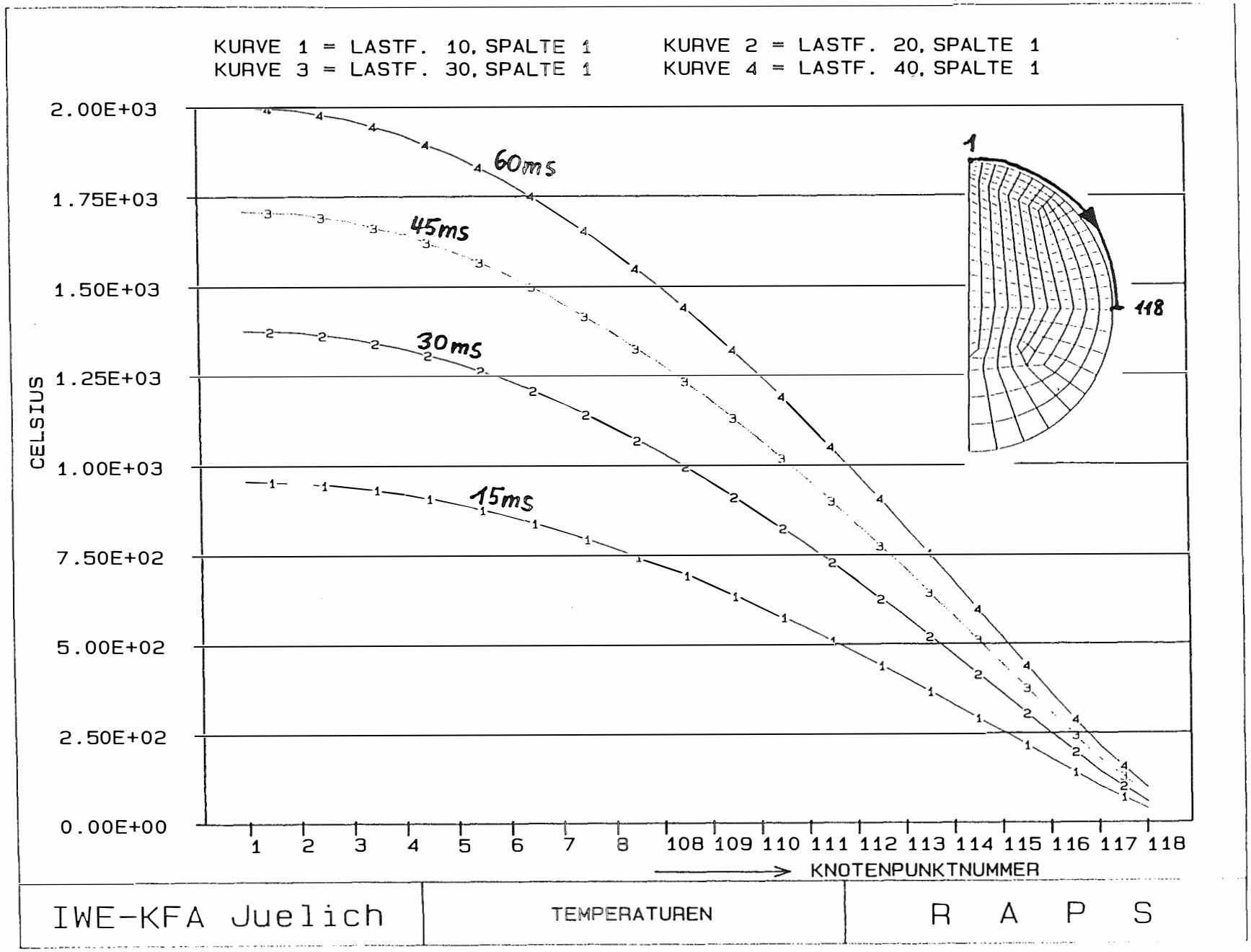
KURVE 1 = LASTF. 10, SPALTE 1
KURVE 2 = LASTF. 20, SPALTE 1
KURVE 3 = LASTF. 30, SPALTE 1
KURVE 4 = LASTF. 40, SPALTE 1
2.00E+03
1.75E+03
1.50E+03
1.25E+03
1.00E+03
7.50E+02
5.00E+02
2.50E+02
0.00E+00
CELSIUS
60ms
45ms
30ms
15ms
1
118
1 2 3 4 5 6 7 8 108 109 110 111 112 113 114 115 116 117 118
KNOTENPUNKTNUMMER
IWE-KFA Juelich
TEMPERATUREN
R A P S

8. FIGURE

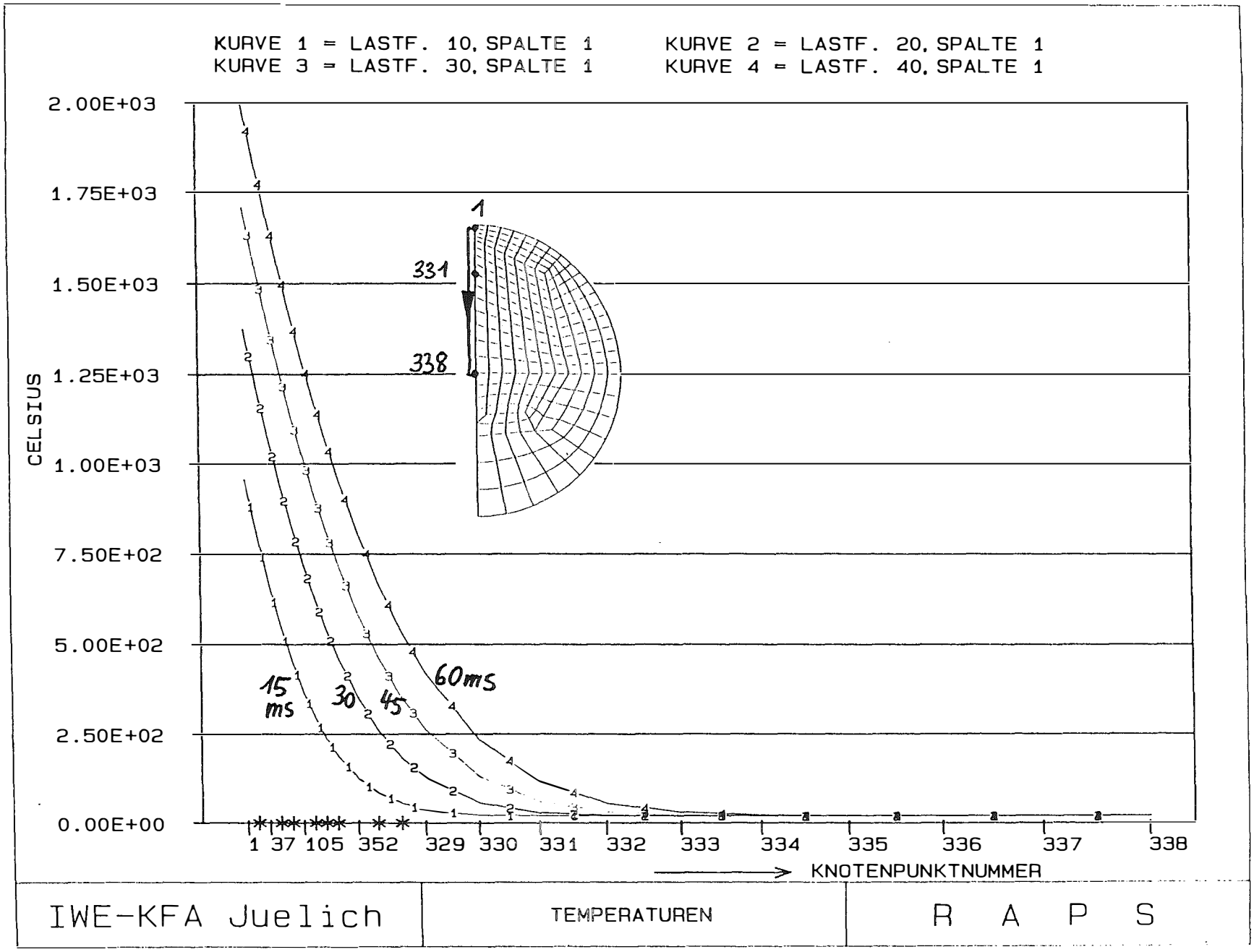
KURVE 1 = LASTF. 10, SPALTE 1
KURVE 2 = LASTF. 20, SPALTE 1
KURVE 3 = LASTF. 30, SPALTE 1
KURVE 4 = LASTF. 40, SPALTE 1
2.00E+03
1.75E+03
1.50E+03
1.25E+03
1.00E+03
7.50E+02
5.00E+02
2.50E+02
0.00E+00
CELSIUS
1
331
338
15 ms
30
45
60ms
1 37 105 352 329 330 331 332 333 334 335 336 337 338
KNOTENPUNKTNUMMER
IWE-KFA Juelich
TEMPERATUREN
R A P S

9. FIGURE

Aufheizung einer Kugel

Maximaler Ausnutzungsgrad einer Kugel bei homogener Aufheizung bis T_{max}

$$\overline{Q} = \frac{4}{3} \pi R^3 \rho c \, (T_{max} - T_o)$$

Ausnutzung bei inhomogener Heizung, Begrenzung durch lokales Erreichen von T_{max} nach einer Zeit t_{krit}

$$Q = q \, \pi R^2 \, t_{krit}$$

Ausnutzungsverhältnis $\eta = Q/\overline{Q}$

$$\eta = \frac{3}{4} \, \frac{1}{R \rho c} \, \frac{q \, t_{krit}}{T_{max} - T_o}$$

mit t_{krit} als Funktion von Stoffwerten etc. unter "Wärmestaubedingungen":

$$\eta \approx 0{,}59 \, \frac{\lambda}{q} \, \frac{T_{max} - T_o}{R}$$

Für 1 cm SiC-Kugeln (λ = 20W/mK, $T_{max} - T_o$ = 1500 K, q = 50 MW/qm):

$$\eta \approx 7\ \%$$

10. FIGURE

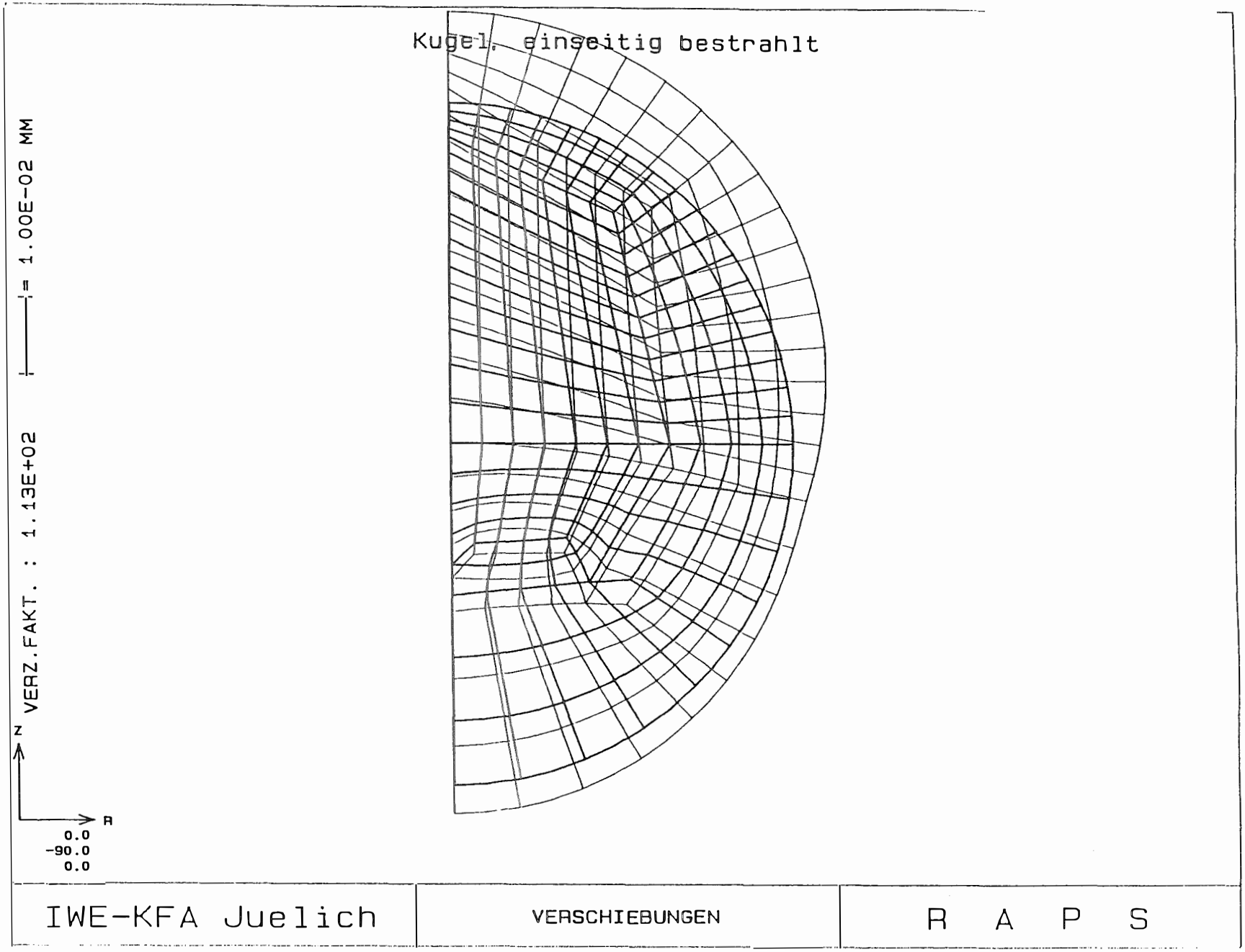
Kugel, einseitig bestrahlt
= 1.00E-02 MM
VERZ.FAKT. : 1.13E+02
Z
R
0.0
-90.0
0.0
IWE-KFA Juelich
VERSCHIEBUNGEN
R A P S

11. FIGURE

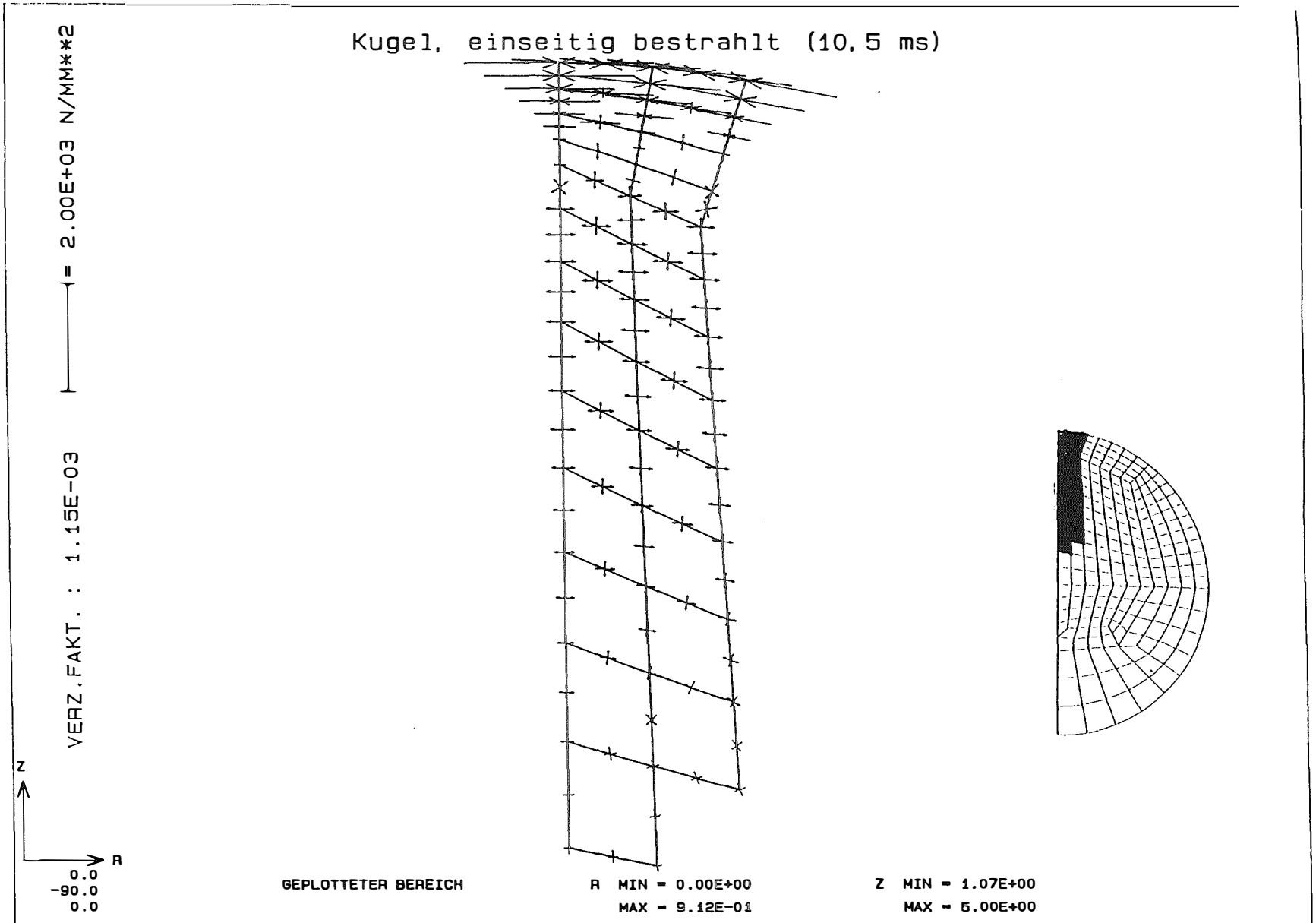

IRW-KFA Juelich	HAUPTSPANNUNGEN	R A P S

12. FIGURE

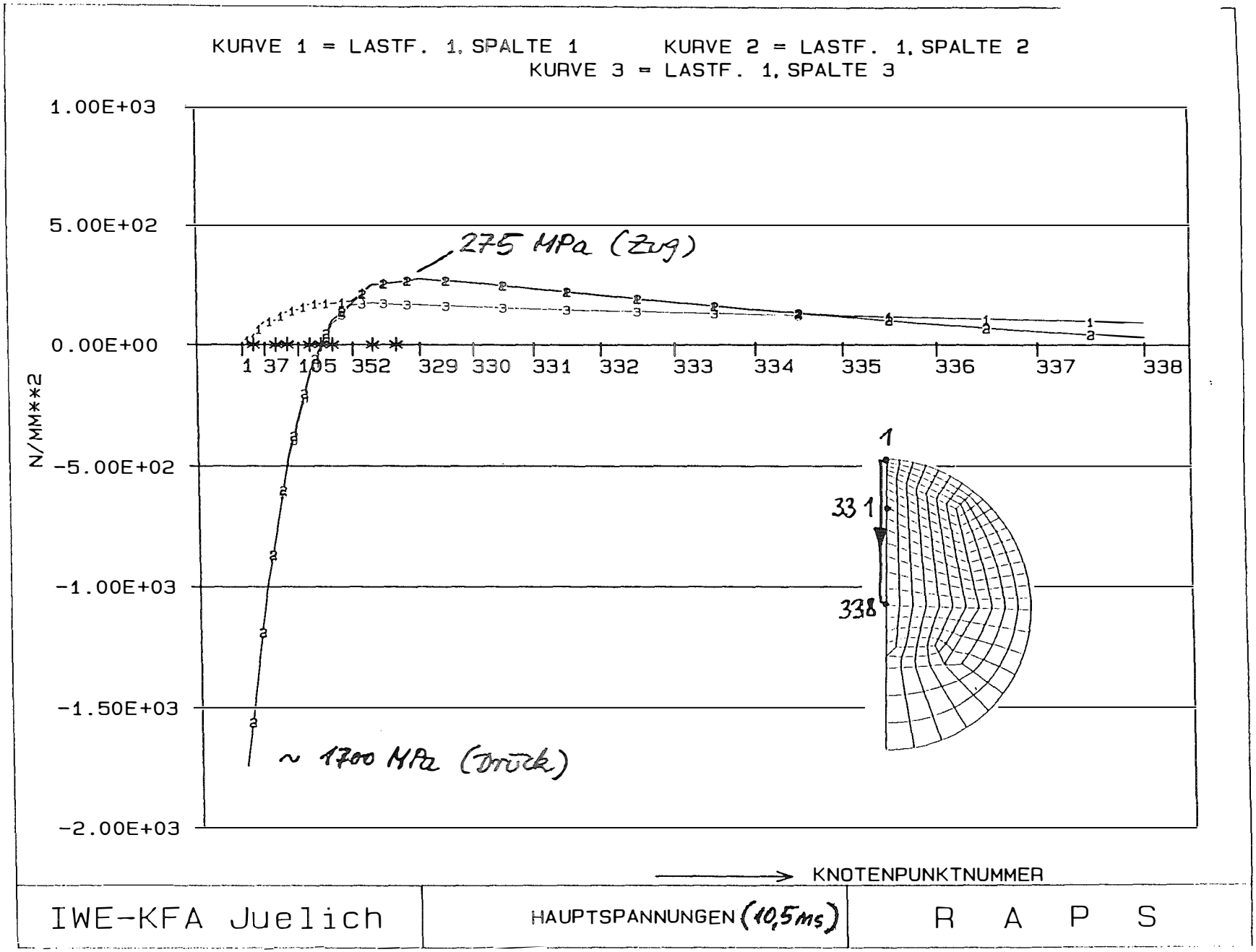
KURVE 1 = LASTF. 1, SPALTE 1
KURVE 2 = LASTF. 1, SPALTE 2
KURVE 3 = LASTF. 1, SPALTE 3
1.00E+03
5.00E+02
0.00E+00
-5.00E+02
-1.00E+03
-1.50E+03
-2.00E+03
N/MM**2
275 MPa (Zug)
~ 1700 MPa (Druck)
1 37 105 352 329 330 331 332 333 334 335 336 337 338
1
331
338
KNOTENPUNKTNUMMER
IWE-KFA Juelich
HAUPTSPANNUNGEN (10,5ms)
R A P S

13. FIGURE

Reibungskräfte bei Rollen im Verband

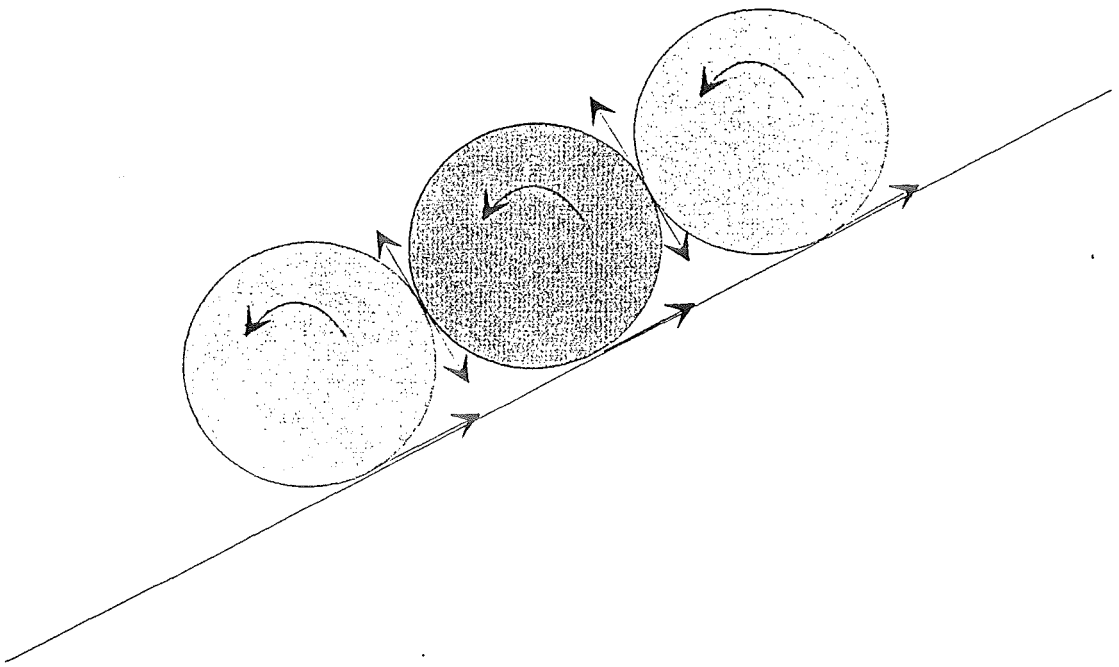

Die Haftreibung zwischen Rollobjekt und Ebene bewirkt ein Drehmoment, das dem Moment, das durch Reibung zwischen den Objekten verursacht ist, entgegenwirkt.

5. Helium release from solid SiC (P. Jung)

Abstract

The literature on helium release from siliconcarbide is reviewed. No results are available on release behaviour of helium implanted to surface near regions. Helium produced in the bulk of SiC is completely released only at temperatures above 2000°C.

Introduction

Plasma facing materials in a future fusion reactor are subject to intense fluxes of helium atoms from three origins:

1) thermalized (10^8 K) ions from the plasma with energies below 10 keV with mean ranges R $\leq$0.078 μm in SiC,
2) α particles from the (D,T) reaction with maximum energies of 3.5 MeV corresponding to R $\leq$9.5 μm and
3) helium produced in the material by (n,α) reactions with energies around 5 MeV, i.e. R $\approx$16.4 μm.

In structural materials, having thicknesses in the cm range, only the last process causes damage in the bulk, while the first two affect only the surface region.

For a variety of metals it is well known that helium causes severe embrittlement at elevated temperatures, mainly by the formation of bubbles along grain boundaries. If this is also the case for ceramics, retention of helium may pose severe limitations to their application at high heat loads.

Results

Investigations by transmission electron microscopy (TEM) of Boron doped SiC after irradiation in a nuclear reactor to doses of $6x10^{24}$ n/m^2, corresponding to helium concentrations around 2000 appm, showed formation of bubbles after annealing to temperatures above about 1200°C [1]. On the other hand implantation of 12 keV He ions at room temperature to doses above 10^{21} He/m^2 caused amorphization and bubble formation in the amorphous region [2]. The formation and growth of such bubbles as observed by TEM indicates helium mobility. But so far no detailled investigations on time and temperature dependence of bubble sizes and growth rates were performed, which could give quantitative results on diffusion and release behaviour. Aside from more qualitative investigations on the formation and growth of helium bubbles [2-5], there are only two investigations on helium release from SiC, one after reactor irradiation [1,6] and one during implantation of α particels [7].

In Ref.[1] helium release from 0.1%B doped SiC powder and from ceramic material (sintered to 98% theoretical density) were measured after reactor irradiation at 650°C with thermal helium desorption spectroscopy (THDS). Figure 1 shows that helium release from the powder (grain size 1.2 μm) occured at much lower temperatures than from the ceramic (grain size $\approx$5 μm). The ceramic specimen was

a plate of 0.15 mm thickness. A ceramic piece of 2 mm thickness showed essentially the same release behaviour at temperatures up to ≈1800°C. This indicates that up to this temperature released helium comes mostly from surface near regions.

Figure 2 [6] shows fractional helium retention as a function of irradiation temperature for ceramic plates of 25x4x2 mm which were grinded to powder before THDS analysis. A comparison of Figs.1 and 2 shows that retention at a given temperature is significantly reduced when this temperature is already applied during irradiation, i.e. during helium production.

When α particles are implanted at low fluxes and elevated temperatures, diffusion coefficients D can be derived from the time evolution of helium release during implantation and its dependence on implantation depth. For He in SiC (3.1 g/cm^3, 90% hexagonal SiC, 10% free Si) at temperatures from 600°-800°C D can be described by [7]:

$$D[m^2/s] = 1.1 \times 10^{-6} \exp(-1.14/kT)$$

Figure 3 compares diffusion coefficients of SiC to those of graphite and copper. In this type of experiments only part of the helium is freely diffusing out of the specimen while a fraction is retained which depends on implantation depth and temperature. The retained helium is released only at a much lower rate and higher activation energy (≈1.8 eV), which also depends on annealing treatment. For implantation or post-implantation annealing at 1000 K, the fractional release rate can be described by [7]:

$$dc/(c\ dt)[1/s] = 1.4 \times 10^5 \exp(-R/32 - 1.8/kT)$$

where R[μm] is the distance from the nearest surface.

Conclusions

1) The presently available quantitative measurements on helium release from SiC simulate helium production in the bulk by (n,α) processes.

2) The results show complex and not well understood dependences of helium release on specimen geometry [1] and annealing [7].

3) The dependences of helium release on temperature and implantation depth imply complex trapping and detrapping processes, probably with simultaneous changes of the trap structure, e.g. by bubble growth.

4) Temperatures of at least 2000°C are needed to completely release helium from the bulk of SiC. Whether or not this temperature is significantly reduced for release from surface near regions as in graphite has not yet been investigated. Also other ceramic materials, e.g. Al_2O_3 showed helium retention up to very high temperatures, while Si and SiO_2 show higher permeability for helium also under irradiation [8].

References

[1] K.Sasaki, T.Yano, T.Maruyama and T.Iseki, J.Nucl.Mater. 179-181 (1991) 407
[2] K.Hojou, S.Furuno, K.N.Kushita, H.Otsu and K.Izui, J.Nucl.Mater. 191-194 (1992) 583
[3] K.Hojou and K.Izui, J.Nucl.Mater. 133&134 (1985) 709

[4] K.Hojou, S.Furuno, H.Otsu, K.Izui and T.Tsukamoto, J.Nucl.Mater. 155-157 (1988) 298
[5] R.B.Wright, R.Varma and D.M.Gruen, J.Nucl.Mater. 63 (1976) 415
[6] K.Sasaki, T.Maruyama and T.Iseki, J.Nucl.Mater. 168 (1989) 349
[7] P.Jung, J.Nucl.Mater. 191-194 (1992) 377
[8] P.Jung, REI-7, Nagoya, t.b.p. in Nucl.Instr.Meth.

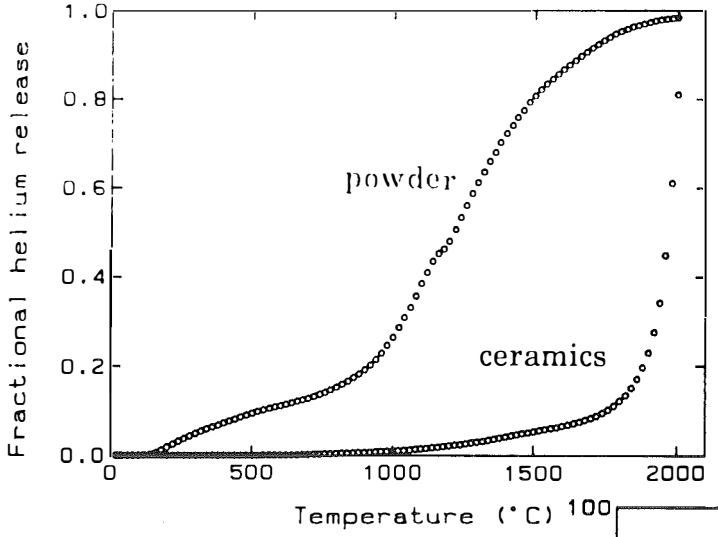

Fig.1.
Fractional helium release from neutron irradiated SiC-0.1%B ceramics (2x4x0.15 mm^3) and powder during heating at 8°C/min. The irradiation temperature was 650°C, neutron dose $6x10^{24}$ n/m^2, giving a helium concentration of about 2000 appm.

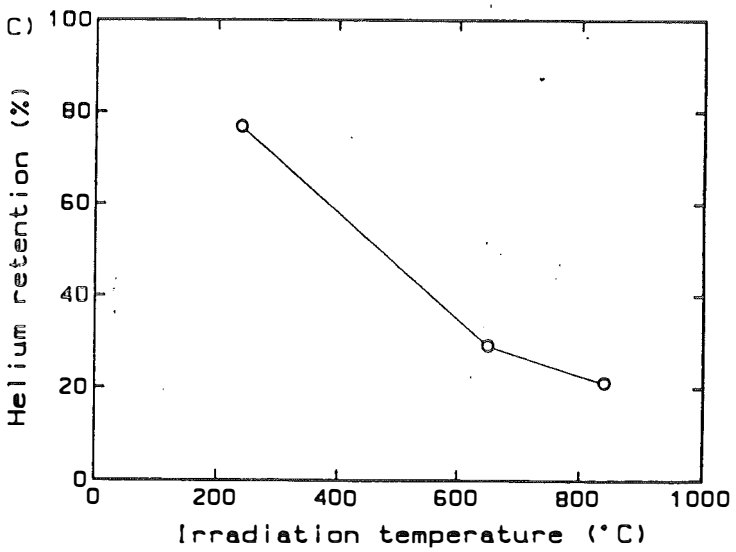

Fig.2.
Fractional helium retention from neutron irradiated SiC (2x4x25 mm^3, grinded to powder after irradiation) as a function of irradiation temperature

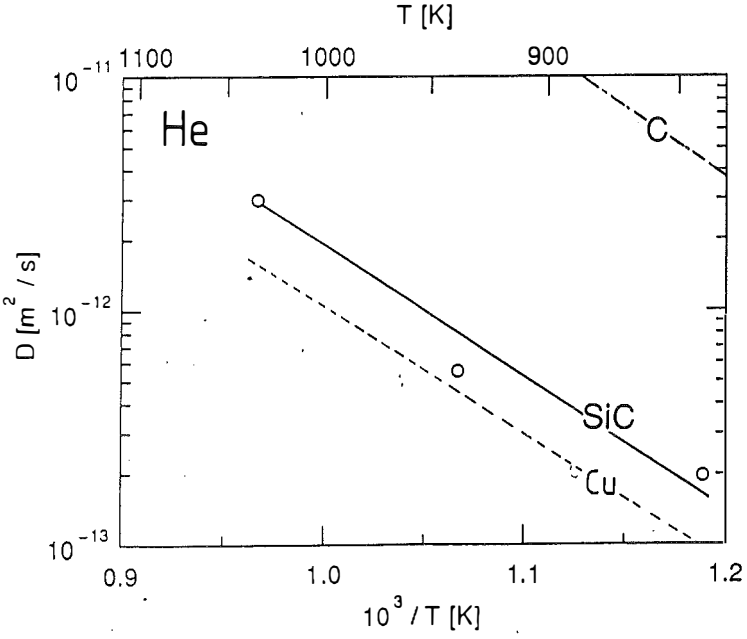

Fig.3.
Diffusion coefficients of helium in SiC as a function of reciprocal temperature, compared to graphite and copper.

6. Rotating targets for power exhaust (V. Philipps)

Introduction:

The main advantages of the concept of fluid targets are:

- absorption of the deposited power via the heat capacity of the fluid and transport of the heat by transport of the fluid out of the heat deposition area. The heat absorption capacity is determined by the velocity of the fluid the heat capacity of the fluid and the maximum allowable surface temperature of the fluid

- no lifetime problem due to target-erosion,

- no problems with mechanical structure of the targets (such as swelling, cracking, fatigue, embrittlement etc.),

- possibility of new particle exhaust techniques (?).

The main problems of using liquids for heat exhaust in fusion devices have been identified so far to be the large induced forces due to interaction the magnetic field of induced currents in the liquid with the magnetic field of the plasma. These forces can be as large as 10 times the gravity force and will cause the fluid to be sprayed over the chamber walls. Further large problems are the pumping of the liquid and the compatability of the liquid with the solid material of the pumping tubes.

A possible solution of the MHD problem might be the use of small liquid droplets which will reduce the force significantly (Mirnov et al, russian concept). A similar idea is the use of small solid spheres. The sphere-concept, however, suffers from other difficulties such as:

- the energy exhaust of large amounts of spheres,

- the transport of large amounts of spheres (in particular problems arising from broken spheres).

Rotating target concept

The concept of rotating targets is a kind of "hybrid" concept between the liquid concept and that of fixed solids. It tries to retain some of the main advantages of the concept of liquids but offers simultaneously better solutions for the main problems of the liquids which were shortly described above. Basic ideas of rotating targets are the same as for liquids:

- energy absorption via heat capacity of a solid

- energy transport via transport of the solid

- conduction of energy to a water cooled substrate during the time of non-exposure to the plasma.

Some model specifications

Fig 1 illustrates some basic assumption of the concept. CFC carbon tiles are used as plasma exposed material. Heat conductivity is assumed to be 200W/mK. The tiles are 2cm thick and fixed via bolts to a water cooled subtstrate.To increase the heat transfer to the substrate a papyex layer between the metal and the CFC is used. The heat transfer time to the metal is a critical point. Bad heat contact ,however, will increase the tile temperature which itself will increase the heat flow to the substrate since heat flow is proportional to ΔT between the tile and the substrate. Maximum tile temperatures well above 1000°C (up to 1800°C) should be possible.

Power flux:	50 MW/m^2
width of the strike zone:	5cm
velocity of target:	10cm/sec

→ energy deposition of one target during one exposure:

$$Q = 2.4 \text{ kWs/cm}^2$$

→ temperature rise of target after heat exchange (heat transport time in tile for heat exchange about 3-5sec)

$$\Delta T = Q/c*m = 385 \text{ °C}$$

where

c = specific heat of carbon:	1.8 Ws/gK
m = mass of carbon per cm^2 surface:	3.6 g/cm^2

Fig 2 shows the evolution of the surface temperature during the plasma exposure (0.5sec) and afterwards. The temperature rises up to 2000°C.($\Delta T = P * k * t^{0.5}$, with $k = 4.3 \times 10^{-5}$ K/Ws). Fig 3 shows the temperature distribution in the tile at the end of the plasma exposure (t = 0.5 sec). The heat has penetrated only about 0.4cm deep into the tile. After about 3-5 sec, however, the heat is dissipated into the tile.

Fig 4 shows a schematic view of a rotating system. The radius of the wheel is 40cm . With v = 10cm/sec and the circumference of 250cm the total cool down time is 25sec. Within this time the energy must be transfered to the metal substrate. The rotating metal wheel transfers finally the energy onto a fixed water cooled tube. Heat transfer between the rotating metal and the fixed tube should be done by a liquid.

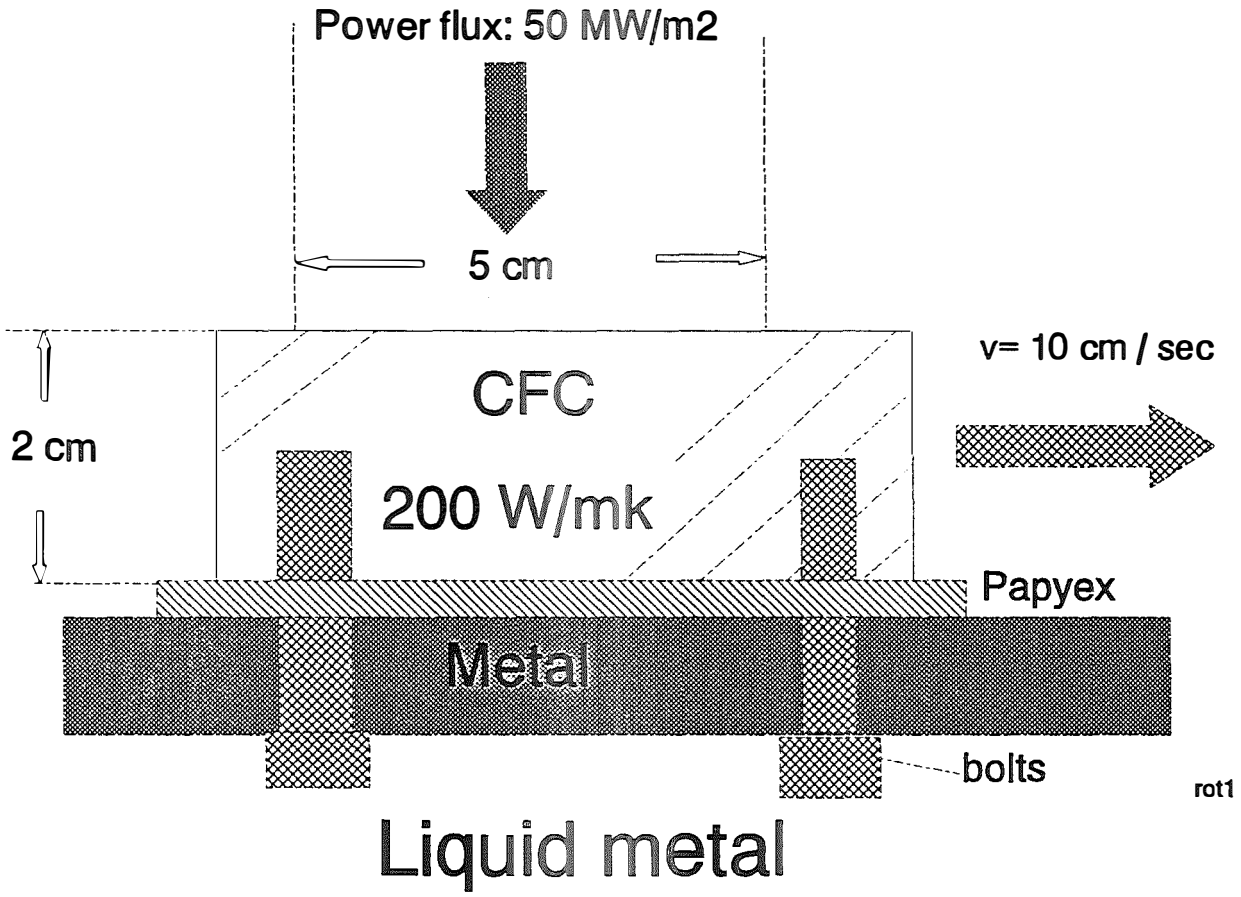

Fig1: schematic view of the rotating target tile arrangement: CFC tile ,2 cm thick (heat conductivity 200W/mK) ,is fixed to a metal substrate via bolts . Papyex is used for better heat transfer.

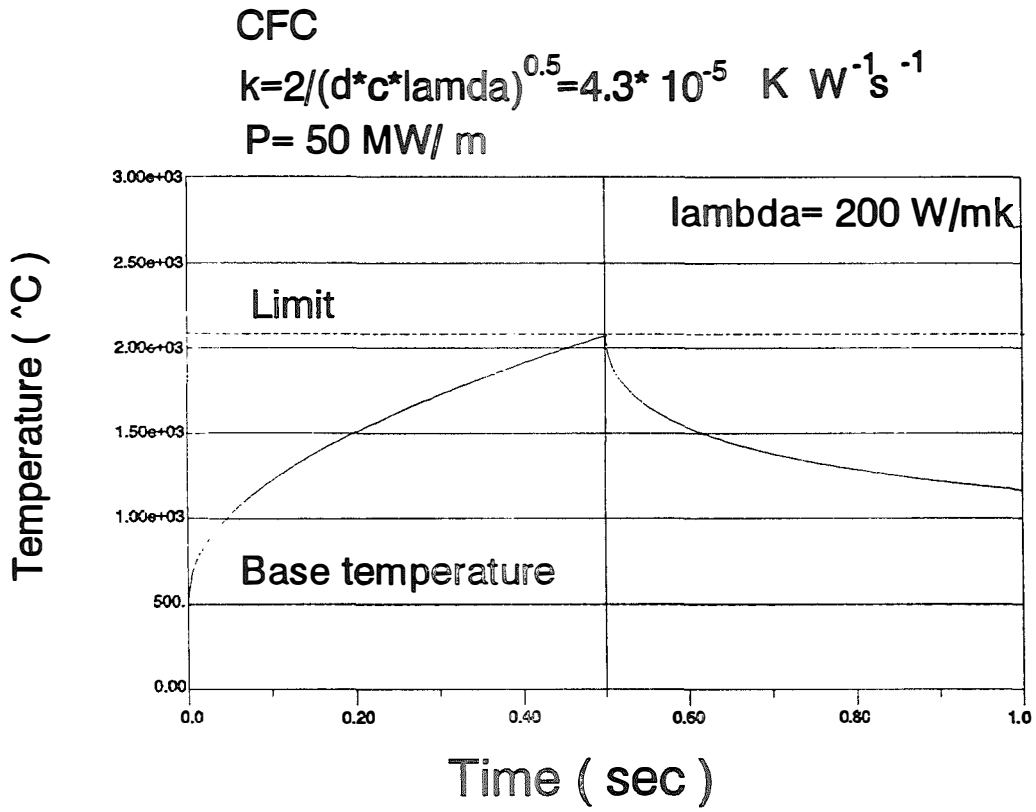

Fig 2: evolution of the surface temperature during exposure (50 MW/m2 for 0.5 sec) and afterwards. Material parameters are indicated.

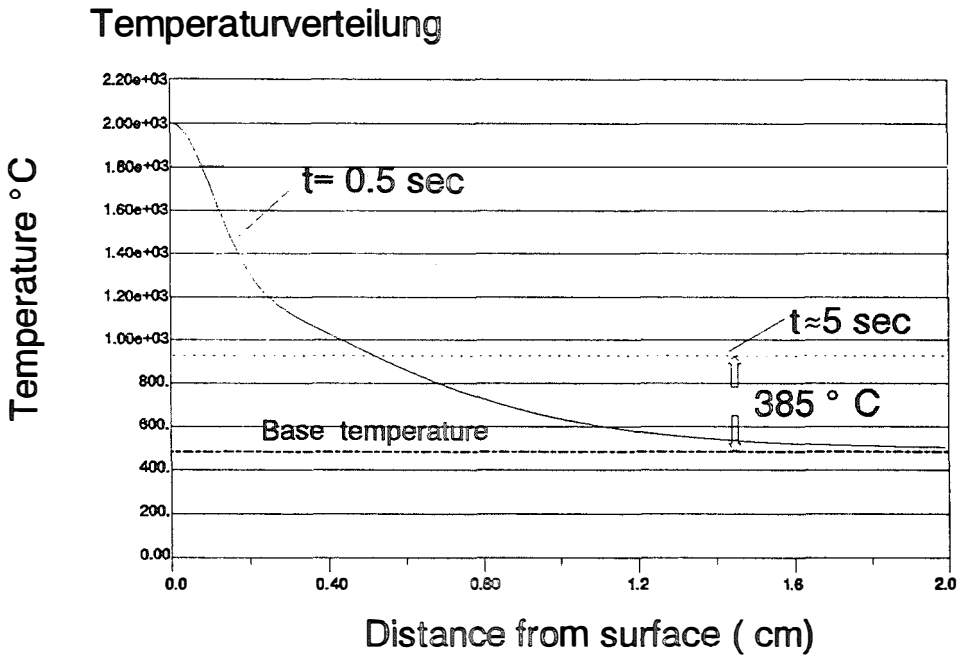

Fig 3: temperature distribution within the CFC tile at the end of the plasma exposure. At t= 5 sec the temperature distribution is uniform. The impinging power is 50 MW/m2 .
The heat diffusivity of the CFC is 0.55 cm2/sec.

7. Rotating,radiation cooled pyrographite target (L. Binkele)

Abstract

The high thermal loads of 50 MW/m^2, which are expected for plasma facing components in ITER, can not be sustained with fixed targets, even if structures, actively cooled with liquids, are used. However, a chance to cope with these extreme heat flux conditions is seen by using movable targets, which were exposed shortly to the plasma radiation and cooled themafter for a longer time to reduce the temperature.

Temperature calculations are reported for radiation-cooled pyrographite segments mounted as high heat flux targets on the periphery of a rotating wheel (1 rps). The wheel is assumed to be exposed on 1/20 of its periphery with a heat load of 50 MW/m^2 and to be radiation cooled on the remaining length. The wheel is considered such that in case of a thermal conductivity of 3 W/cmK average temperatures between 1870 K (plasma facing surface) and 1725 K (rear surface) develop in the pyrographite segments. Heating the segments up to this temperature level occurs within 80 % after 90 sec.

Conceptional considerations

The concept is schematically illustrated in Fig. 1. At those sites of the plasma machine where heat flux has highest intensity (divertor sites) the first wall is replaced by rotating wheels attached from outside. Thus part of the wheel periphery is heated whereas the remaining larger part is radiation cooled within a water jacket system. The part of the wheel which is facing the plasma determines among other properties the temperature level which develops along the wheel periphery after the initial heating-up period. As indicated in Fig. 1 the periphery of the wheel is proposed to have two concentric ceramic layers. The outer layer contains segments of pyrographite, which exhibits a good thermal conductivity, whereas the inner layer has to be made out of a thermally insulating carbon material, e.g. clean carbon bricks. The pyrographite segments should be oriented such that correlation between wheel geometry and crystallography is achieved, i.e. the a-axes are radially and c-axes tangentially oriented. This allows a fast heat transfer in radial direction and a nearly homogeneous temperature distribution in the complete pyrographite material. The pyrographite orientation also provides a large radiation source during the cooling cycle and

thus a decrease in temperature is achieved. However, the temperature should not be to low, in order to keep lattice damage and reduction of thermal conductivity by fast plasma neutrons as low as possible. Experience with changes in thermal conductivity of graphitic materials due to neutron irradiation favours a service temperature above 1300°C. The bad thermal conductivity of the inner carbon layer is considered to protect the shaft of the wheel from the high temperatures.Because of the high degree of lattice disorder in such materials a significant change of thermal conductivity is not very likely despite of the low temperatures. Moreover, an increase in defect density would increase the insolation effect, i.e. the service behaviour would be improved.

First calculations to estimate feasibility

Fig. 2 magnifies a segment of the wheel periphery showing the pyrographite on top of the carbon insulation. The stated dimensions were chosen to get an idea of the obtainable equilibrium temperature. The thermal conductivities of pyrographite and carbon insulation were assumed to be infinity and zero, respectively. Note that a more realistic case with 3 and 0,015 W/cmK is considered in a second step. The front surface of the pyrographite segment is facing a plasma heat flux of 50 MW/m^2 = 5 KW/cm^2. If the wheel periphery has a length of 5 m (wheel diameter 1,59 m) and the plasma facing part is 1/20 of the periphery (= 25 cm) then an individual segment absorbs an energy of 10^3 Wsec (5 KW/cm^2 x 4 cm^2 x 1/20sec) during one revolution*. This energy would cause in case of negligible heat radiation of the pyrographite segment an increase in temperature by

$$\Delta T_{Heating} = \frac{1O^3\ (Wsec/sec)}{V_{Seg.} \cdot d \cdot C_p\ (Wsec/K)}\ ,\ \frac{K}{sec}$$

$V_{Seg.}$ = 2 x 2 x 4 cm^3

d = 2,2 g/cm^3

C_p = 0,71 (at 300 K) to 2,09 (at 2600 K) $\frac{Wsec}{gK}$ [4)]

During one rotation the heat loss by radiation is small in the low temperature regime and approaches in the high temperature regime at equilibrium temperature an equivalent to $\Delta T_{Heating}$. Following Boltzmann's radiation law with the emissivity $\varepsilon \approx 0,8$ and the segment surface A capable of radiation - front surface (4 cm^2) and two of the four side surfaces (2 x 8 cm^2) - a cooling effect of

---

* The wheel diameter has no direct influence on the outcome of the above calculation other than it influences the size of the plasma facing first wall window.

$$\Delta T_{Cooling} = \frac{A \cdot \varepsilon \cdot 5{,}77 \cdot 10^{-4} \left[\left(\frac{T}{100}\right)^4 - \left(\frac{300}{100}\right)^4 \right] \text{(Wsec/sec)}}{V_{Seg.} \cdot d \cdot C_p \text{ (Wsec/K)}}, \quad \frac{K}{sec}$$

T: absolute temperature in K

is obtained within one rotation. The relation assumes that the radiation hits a black cooling element kept at 300 K.

Summing up the differences $\Delta T_{Heating} - \Delta T_{Cooling}$, the temperature rise within a pyrographite segment can be calculated successively during the initial heating up period. The resulting functional dependence (Fig. 3) approaches asymtotically the limiting value of 1815 K. The raise in temperature from 300 K to 1815 K under conditions of pulsed heat flux is obtained within 80 % after 90 sec and within 99 % after 180 sec. At the equilibrium temperature (1815 K) a saturation heat flux density of about 50 W/cm^2 must be assimilated by the cooling systems, which is 1 % of the heat flux density hitting the plasma faced surface of the pyrographite segments. If the cooling systems are water cooled with a flow velocity of 1-2 m/sec, a temperature decrease of 50 K can be estimated in the interface assuming a heat transfer coefficient of 1 W/cm^{2}K. The water in a cooling circuit would warm up by 40 K (1,5 l/sec flow rate).

Now the question is how properties change when more realistic values are taken for the thermal conductivity along the a-axis of the pyrographite segments. Fig. 4[5] summarizes high temperature thermal conductivities reported in literature. Taylor[6] obtained with pyrolythic graphite, annealed under pressure at 3000 K values between 5 W/cmK at 900 K and 3.2 W/cmK at 2000 K. The latter value was determined following a special fitting procedure suggested by the author. A similar materials is processed by Le Carbone Lorraine in plates of 6 x 4 x 0,5 cm^3 (so called pseudo single crystals)[7].

Fig. 5 shows the decrease of thermal conductivity by fast neutron irradiation in the high temperature regime. Projection of the data to the conditions of ITER with fast neutron fluences around of 10^{21} cm^{-2} at irradiation temperatures of ≈1500°C indicates that the decrease of thermal conductivity is more or less negligible.

Concerning the carbon insulation a refinement from zero thermal conductivity to realstic values is less significant. A high strength is not necessary, i.e. porosity can be large and thermal conductivities in the order of 0,015 W/cmK can be assumed being not unrealistic. Note that the temperature dependence of thermal conductivity is typically small in such materials. The above value is still so small that the interface between the pyrographite segment and the carbon insulation can be considered to be adiabatic for the future.

The important question that needs an answer refers to the temperature fluctuations in a pyrographitic segment during one revolution of the wheel. The thermal conductivity now will be treated as being constant with a value of 3 W/cmK. An exact mathematical analysis of this problem is not trivial and requires extended calculation efforts. Thus only an approximate procedure will be outlined next. However, it will allow a sufficiently precise limitation of the actually occuring temperature fluctuations.

The temperature gradient which develops under the influence of the plasma beam in z-direction was determined by finite element calculation. The differences in temperature along the y-directions were neglected (Fig. 2). The temperature was varied at the plasma facing surface of the pyrographite segment assuming a mean heat load of 1 kW (5 KW/cm^2 x 4 cm^2 x 1/20 sec = 1000 Wsec per revolution, i.e per sec). The correct surface temperature is obtained when the summ of heat losses from the plasma facing surface and the other free surfaces of a segment just compensates the heat load of 1 KW approaching the lowest element at the interface to the carbon insulation. As a solution a surface temperature of about 1870 K and a temperature decrease within the segment of 145 K were determined. The graphical representation of the temperature curve inside the segments is shown in Fig. 6 (open circles).

However, in reality the average heat load of 1 KW consists of individual pulses with 20 KW height, 50 msec width and a frequency of 1 Hz. Thus also temperature pulses around the averaging curve in Fig. 6 must be considered. The amplitudes are highest close to the plasma facing surface of the segment and decrease towards the interface with the carbon insulation. Estimatations yielded fluctuations between 1815 K and 2159 K at the surface[10-13] which diminish to a few degrees in a depth of 2 cm.

As the time dependence of the heat flux is periodic but not harmonic the temperature-amplitudes at z = 0 are 55 K (negative) and 289 K (positive)[13]. Temperature peaks (z = 0) reach 2159 K but are only short lasting, as demonstrated in Fig. 6 by the curve for t = 100 msec. A high rotation speed would keep the average power of 1 KW unchanged but would decrease the temperature fluctuations and would increase damping of the temperature waves. It is also of importance that the maximum temperatures in pyrographite can be influenced by the dimensions of the segments in y- and z-direction (Fig. 2) . A large z-dimension and a small y-value (normal of the plane of the wheel) yield under otherwise constant conditions lower temperatures.

Design aspects

The separation and spreading of the wheels as indicated in Fig. 1 is of specific importance because the cooling jackets can be arraged close to the window in the wall of the plasma machine. The side part of the cooling element, closest to the window should be made out of a massive, not water cooled plate to safe space and thus to approach the heat flux loaded periphery as close as possible. Close to the shaft the further separated position of the wheels should provide enough space for bearing and driving gear. To safe space also universal joints rather than individual driving gears seem possible.

Joining of the pyrographite segments and the insulating carbon parts with the wheel should allow thermal expansion and should transfer only little heat into the metallic structure of a wheel. Possibly carbon fibres would be appropriate to tight the components together. They could be fixed in the pyrographite segments and kept under tension by springs close to the shaft. A 2 mm carbon fibre supplied by Carbone Lorraine[7)] has a tensile fracture load of 100 N. The centrifugal force developed in a pyrographite segment at 1 rps is in the order of 1,2 N.

References

1) L. Binkele
Thermal conductivity of neutron-irradiated graphites at temperatures between 50 and 1000°C
High Temperatures - High Pressures, 1972, Vol. 4, p. 401-409

2) L. Binkele
Ein Verfahren zur Bestimmung der Wärmeleitfähigkeit von neutronenbestrahlten Graphiten bei Temperaturen zwischen 50 und 1000°C
Report Jül 1096-RW, 1974

3) L. Binkele
A model of calculating the thermal conductivity of fast neutron irradiated reactor graphites
Journal of Non-Equilibrium Thermodynamics, 1978, Vol. 3, p. 257-266

4) W. Blanke
Thermophysikalische Stoffgrößen, 1989, p. 171, Springer-Verlag Berlin

5) B.T. Kelly in
Chemistry and Physics of Carbon, Editor P.L. Walker, Vol. 5, p. 123, 1969, Marcel Dekker Inc., New York

6) R. Taylor
The thermal conductivity of pyrolytic graphite
Philosophical Magazin, 1966, Vol. 13, p. 157-166

7) Prospectus "Werkstoff Graphit"
Deutsche Carbone A.G., a subsdiary company of Le Carbone Lorraine France, Frankfurt/Main, ~ 1983

8) L. Binkele
Effekt einer Neutronenbestrahlung bei 1450°C auf die Wärmeleitfähigkeit von Feinkorn- und CFC-Graphiten
Technical Notice KFA/IWE-TN-22/93

9) R. Taylor
Thermal conductivity of low density carbon
High Temperatures - High Pressures, 1972, Vol. 4, p. 649-658

10) A.J. Angström
Neue Methode, das Wärmeleitfähigkeitsvermögen der Körper zu bestimmen
Annalen der Physik und Chemie, 1861, Vol. 114, p. 513-530

11) B. Abeles, G.D. Cody, D.S. Beers
Apparatus for the measurement of the thermal diffusivity of solids at high temperatures
Journal of Applied Physicis, 1960, Vol. 31, p. 1585-1592

12) H.S. Carslaw, J.C. Jaeger
Conduction of heat in solids
Reprint of the Sec. Edition (1959), 1980, p. 75, Oxford University Press

13) H.S. Carslaw, J.C. Jaeger
Loc. cit., p. 401/402

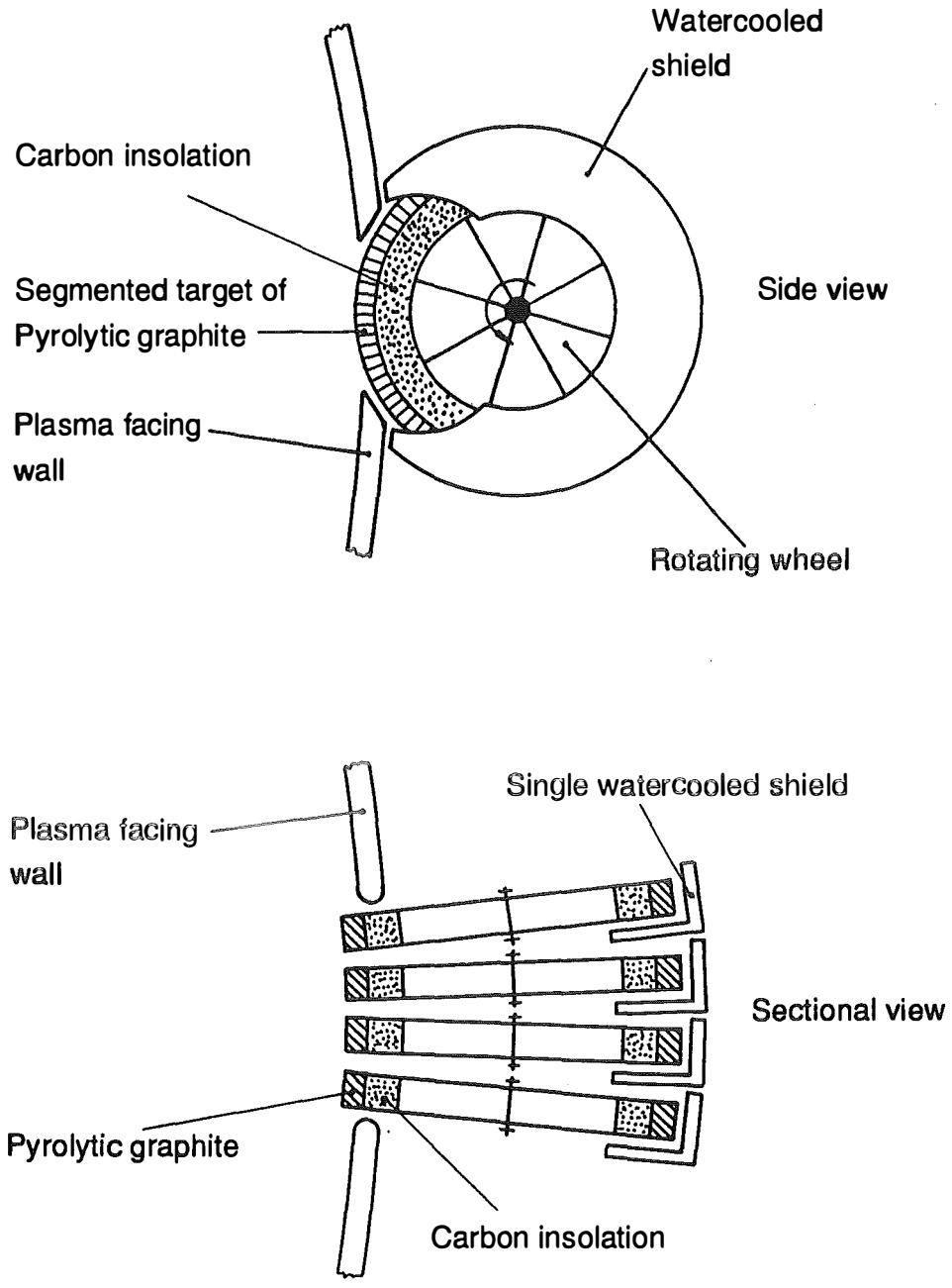

Fig. 1
Schematic drawing of the rotating wheel concept for heat removal. Radiation cooled pyrographite segments mounted on the periphery of the wheel provide the target material.

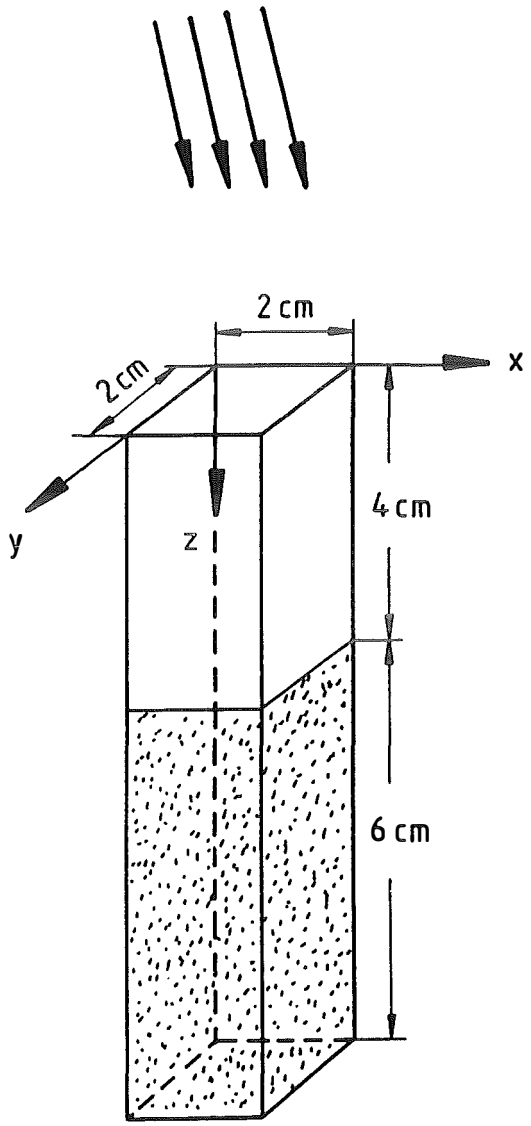

Plasma radiation

Periphery of the wheel (z=0)

Pyrolytic graphite
(a-axis II z, c-axis II x)

Carbon insulation

Fig. 2
Single segment of pyrolytic graphite on top of carbon insulation

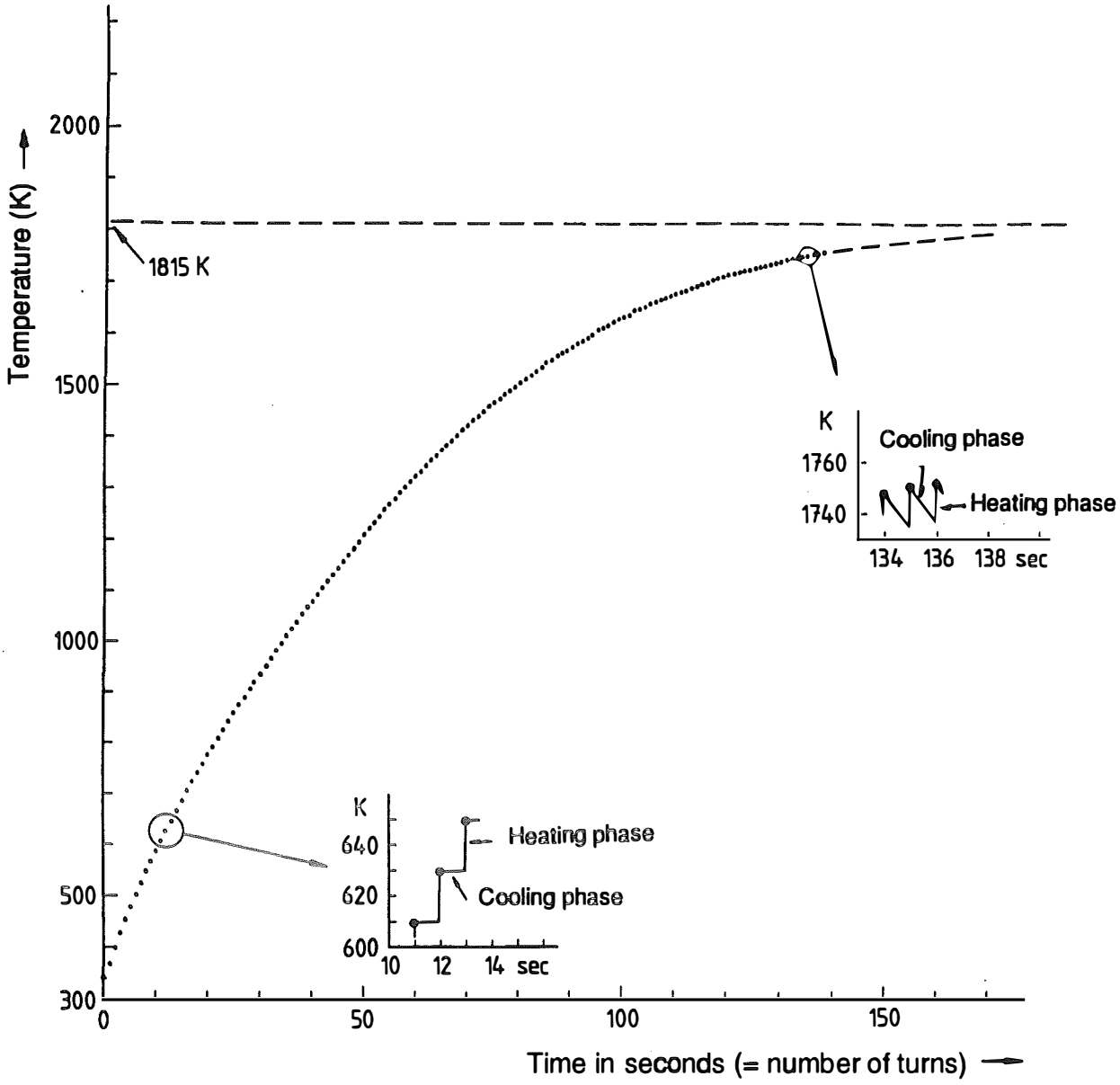

Fig. 3
Temperature increase with time in a pyrolytic graphite segment during the starting period.
The input data for the corresponding calculation are the following:

Volume of pyrolytic graphite segment:	16 cm^3
Emissivity ε:	0.8
Radiation to a black environment of temp.:	300 K
Summation of areas radiating:	20 cm^2
Thermal conductivity of pyrolytic graphite:	∞ ($\gg$10 W/cmK)
Thermal conductivity of carbon insulation:	0 ($\ll$0,1 W/cmK)
Specific heat C_p of pyrolytic graphite:	Polynomials given by Blanke[4)]
Rotary velocity:	1 turn/sec
Duration of heat puls:	1/20 sec = 50 msec
Energy of heat puls:	10^3 Wsec

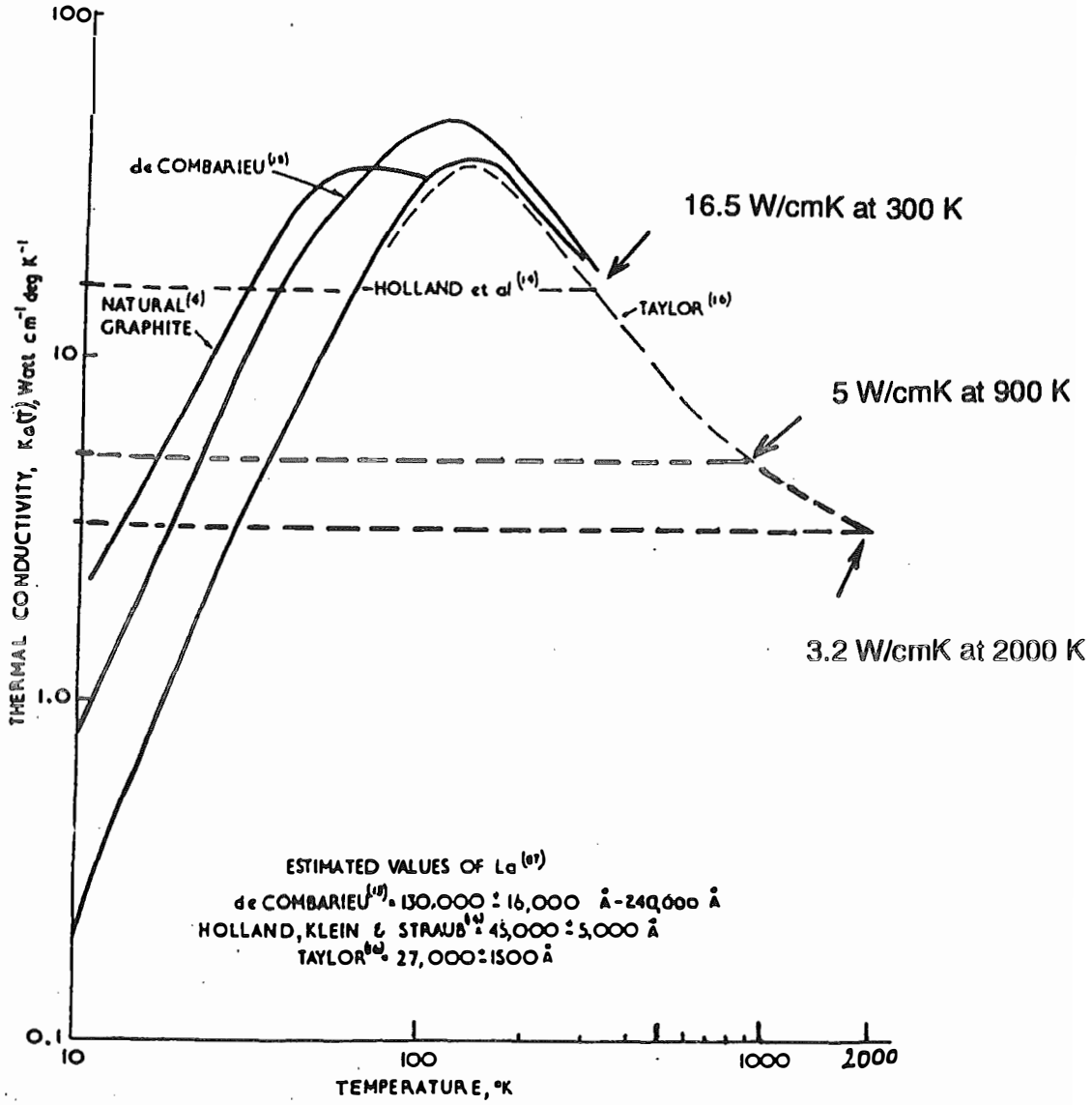

Fig. 4
Thermal conductivity data for natural and pyrolytic graphite compiled by Kelly[5]. The Taylor curve for pyrolytic graphite was extrapolated to temperatures between 900 and 2000 K using a fit-formula given by the author[6].

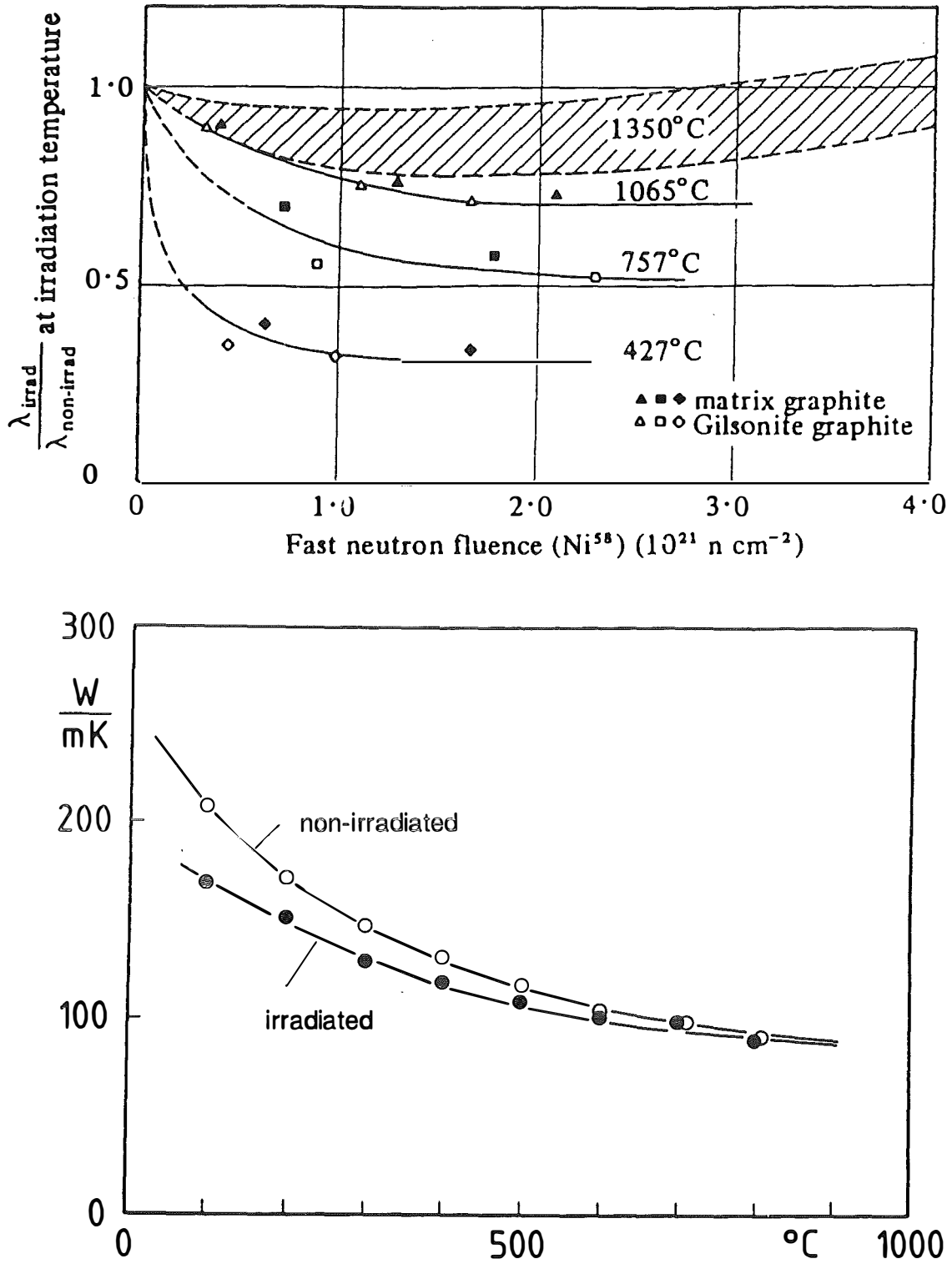

Fig. 5
Thermal conductivity ratio $\lambda_{irrad.}/\lambda_{non\text{-}irrad.}$ at different temperatures (427-1350°C) versus fast neutron fluence for two reactor graphites (upper figure)[1]. Thermal conductivity of a CFC graphite before and after fast neutron irradiation at 1460°C, the dosis amounted to $3{,}8 \cdot 10^{21}$ $cm^{-2} \hat{=} 2{,}8$ dpa (lower figure)[8].

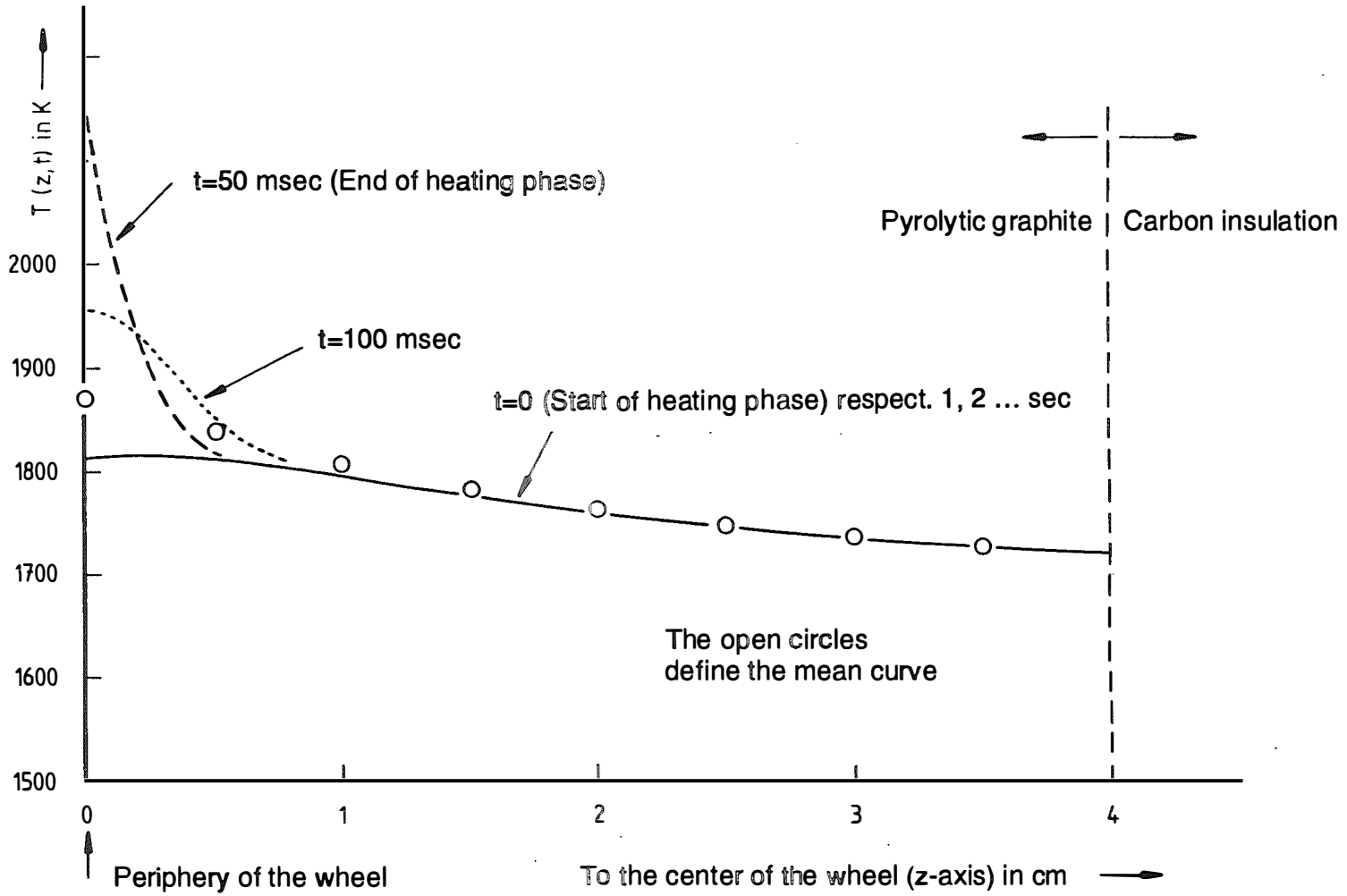

Fig. 6
Calculated temperature profiles for the center line of a pyrolytic graphite segment during one wheel rotation. The basal plane thermal conductivity (parallel to the a-axis) was chosen to 3 W/cmK, while the other parameters were equal to the specifications given in Fig. 3. The open circles define the average values with respect to time of the temperature profiles. Because of the high attenuation of entering temperature waves, the differences between instantaneous and mean temperatures in the range $z > 2$ cm are only small (some dregrees or lower). Contrary to this behaviour the temperature at $z = 0$ increases during the heating phase (50 msec) from 1815 K to 2159 K $\hat{=}$ 344 K and decreases to 1953 K after further 50 milliseconds[13]. The two curves which were plotted for 50 and 100 msec in the range $0 < z < 1$ cm are approximations calculated by the use of formulas, which describe the temperature response after absorption of a single puls in the absence of heat losses at the surface[12].

8. Conveying systems for liquid metals and granular materials (W. Kohlhaas)

Abstract

In large thermonuclear test facilities or in a fusion reactor extremely high thermal loads have to be taken by i.e. divertor chamber walls or by pump-limiter blades.
It has been experienced that the realization of actively cooled wall structures which guaranty a reliable operation over a long time is very difficult.
Therefore the idea was pursued to build such wall structures or limiter blades covered by a flowing mass of a liquid metal or a granular material which is heated up by the thermal load and thus removing the thermal power out of the plasma chamber.
This paper describes conveying systems necessary for the transport of the liquid metal and the granulated material, respectively.

INHALT

Elektromagnetische Flüssigmetallpumpen

Arbeitsweise

Elektromagnetische Induktionspumpen sind eine Sonderform des asynchronen Linearmotors. Auf einem Magnetgestell ist eine Wanderfeldwicklung aufgebracht, die ein entlang des Magnetgestells fortschreitendes Wanderfeld erzeugt. Durch einen magnetischen Rückschluß wird der magnetische Fluß des Wanderfeldes so geführt, daß er an jeder Stelle innerhalb des Pumpenkanals senkrecht zur Fließrichtung des Flüssigmetalls zeigt.

Das Wanderfeld induziert elektrische Sekundärströme im Flüssigmetall, deren Magnetfelder zusammen mit dem erzeugenden Wanderfeld Kräfte auf das Flüssigmetall ausüben (s. Abb. 1).

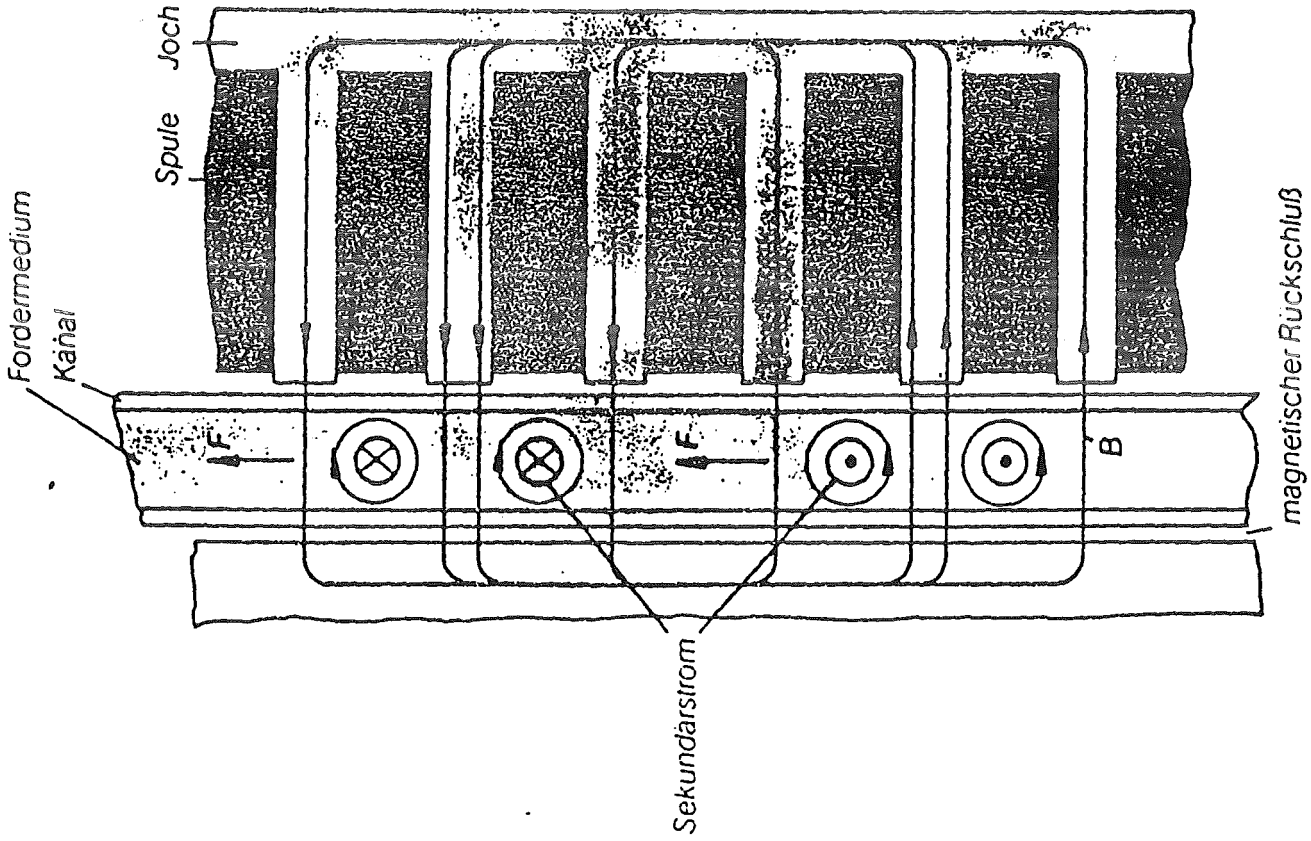

Abb. 1 Prinzip der elektromagnetischen Induktionspumpe

Aufbau

Das Magnetgestell wird durch geschichtete Bleche mit kammförmigem Profil so aufgebaut, daß zum Pumpenkanal gerichtete Spulenkammern entstehen.

In diese werden die Spulen eingebracht und so zusammengeschaltet, daß bei Einspeisung mit Drehstrom ein mit Synchrongeschwindigkeit fortschreitendes Wanderfeld entsteht.

Induktionspumpen werden in verschiedenen Bauformen gebaut (s. Abb. 2):

- Flachkanalpumpen
- Rundkanalpumpen
- Rundkanalpumpen mit innerem Rücklauf und
- Schraubenkanalpumpen.

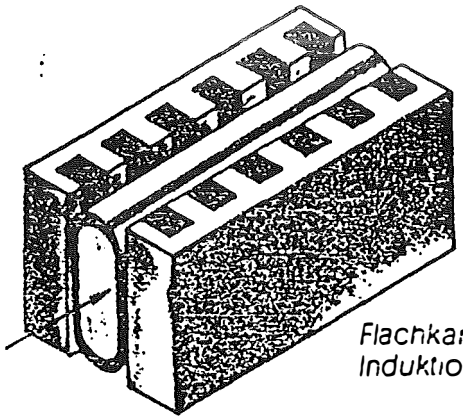

Flachkanal-Induktionspumpen

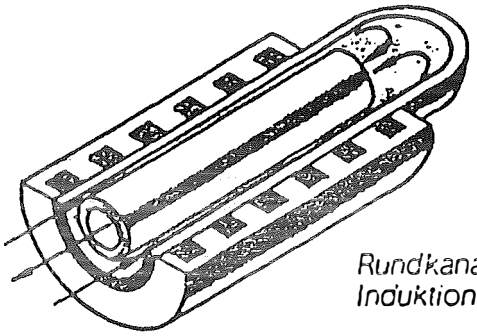

Rundkanal-Induktionspumpen

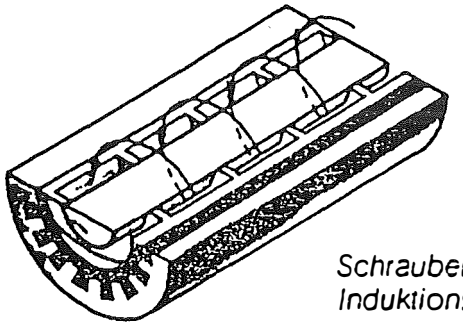

Schraubenkanal-Induktionspumpe

Abb. 2 Bauformen für elektromagnetische Induktionspumpen

Bei Flachkanalpumpen befindet sich der Pumpkanal zwischen zwei Drehstromständern, in denen das Wanderfeld erzeugt wird. Diese Bauart verwendet keinen vom Flüssigmetall umfluteten Rückschluß, so daß diese Bauform bevorzugt bei Anwendungen mit hohen Temperaturen (T > 600 °C) vor allem bei agressiven Flüssigmetallen (z.B. Al und Zn) eingesetzt werden.

Als Beispiel für die Pumpenbaureihe der Flachkanalpumpen werden in Abb. 4 die Förderkennlinien (bei maximalem Spulenstrom) für Aluminium (700 °C) gezeigt. Durch Absenkung des Spulenstromes können geringere Pumpendrücke erreicht werden (Abb. 5).

ABB 4 : Pumpenkennlinien für EM - Pumpen
Aluminium 700 °C

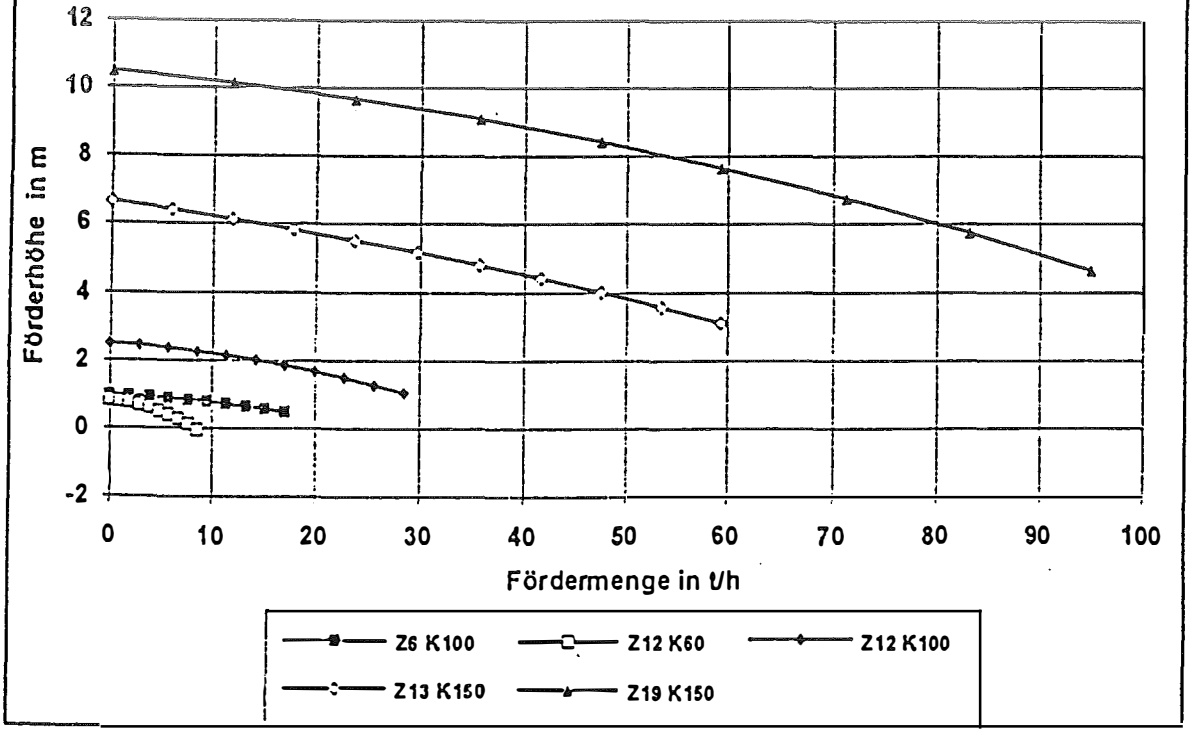

SIEMENS

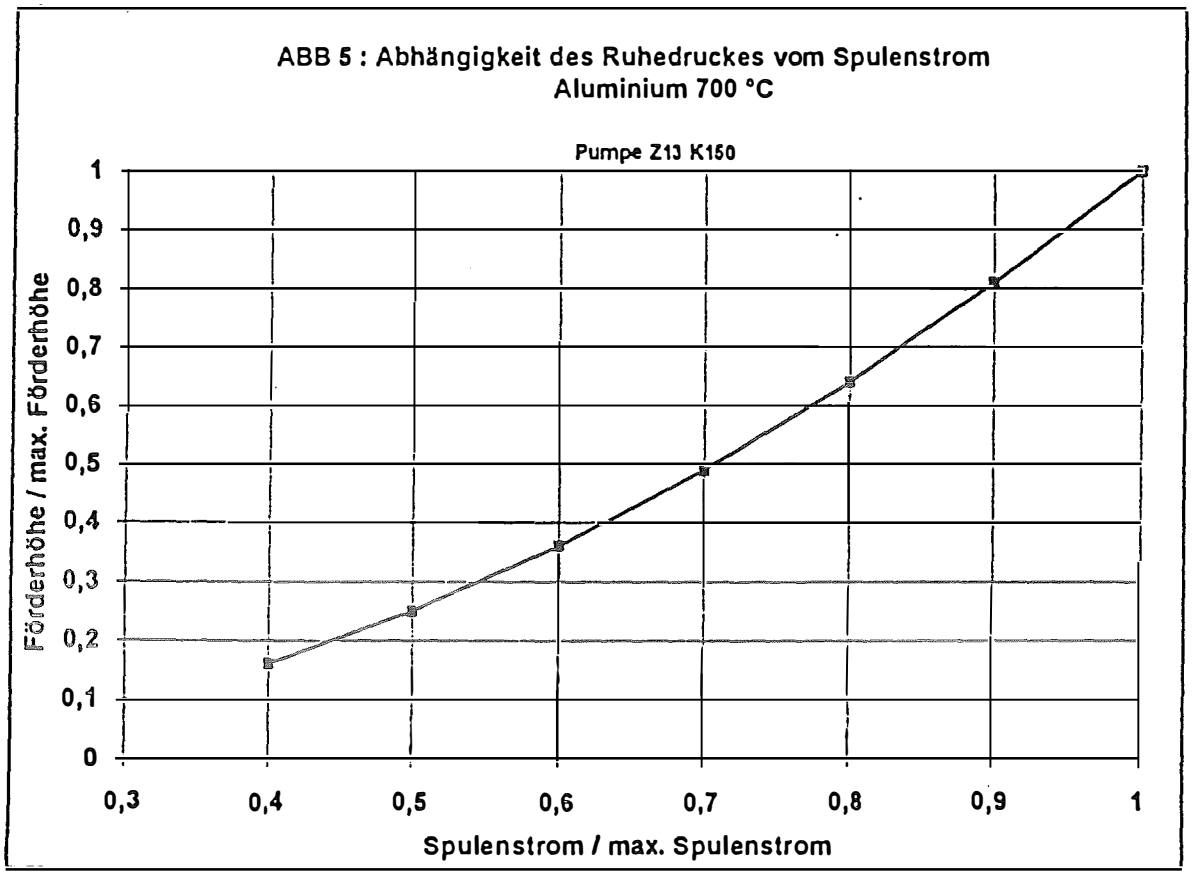
ABB 5 : Abhängigkeit des Ruhedruckes vom Spulenstrom
Aluminium 700 °C
Pumpe Z13 K150
Förderhöhe / max. Förderhöhe
1
0,9
0,8
0,7
0,6
0,5
0,4
0,3
0,2
0,1
0
0,3
0,4
0,5
0,6
0,7
0,8
0,9
1
Spulenstrom / max. Spulenstrom

Kh / 10. 1. 1994

Kreislauf mit flüssigem Aluminium für Limiterfläche von der Größe eines ALT-II Blattes

Volumenstrom, Massenstrom

Breite des Blattes	1,5 m
Dicke der fließenden Alu-Schicht	5 mm (Wt)
Fließgeschwindigkeit	1,5 m/s (Wt)
Volumenstrom	0,011 m^3/s
"	40,5 m^3/h
Massenstrom	113,4 t/h

Gewählte Umwälzpumpe

Siemens AG
KWU NPM3

Typ:

Fluctostat Z 19 K 150

Massenstrom	115 t/h
Förderhöhe bei diesem Massenstrom	2 m

Maße:

Länge	1,2 m
Breite	1,0 m
Höhe	0,4 m
Gewicht	390 kg

Anschlußleistung	330 kVA
Anschlußspannung	3 x 380 V
Leistungsfaktor	0,2
Preis der Pumpe (Größenordnung)	DM

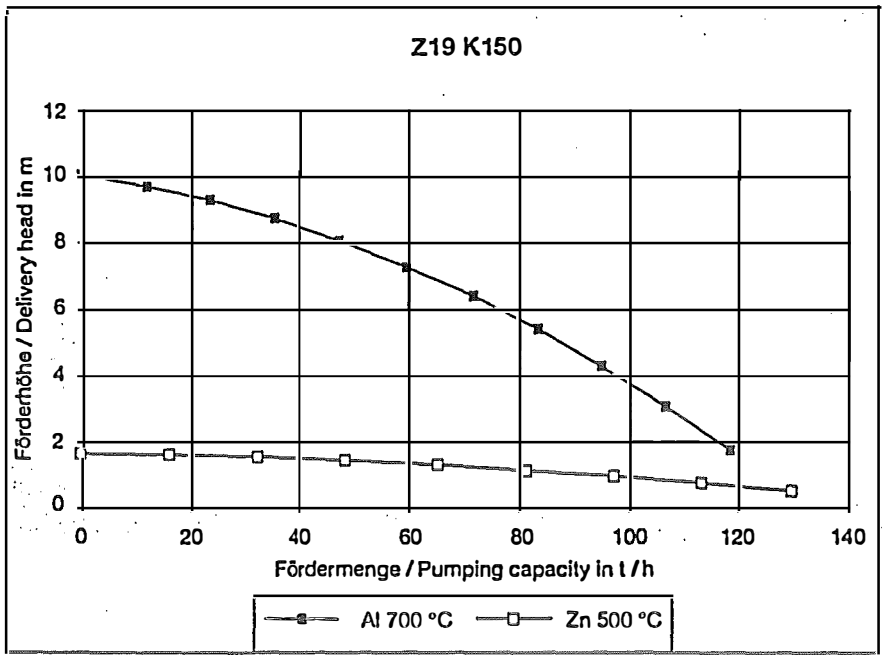

Förderkennlinie bei Nennstrom 240 A
Pump Characteristic at Nominal Current 240 A

Rohrleitungen

Durchmesser der Rohrleitungen	DN 100 oder DN 150

Alle Rohre mit Begleitheizung lieferbar

Wärmetauscher

Wärmetauscher - Bauart unklar

SIEMENS

Liquid Metal Pump

Flüssigmetallpumpe Z19 K150

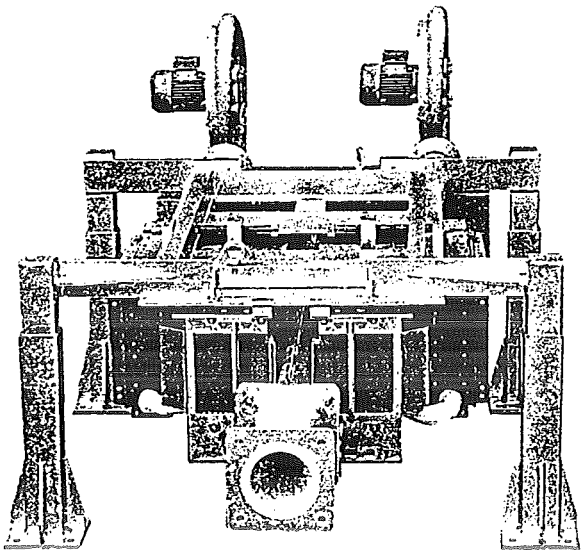

Elektromagnetische Induktionspumpen ersetzen bisher gebräuchliche, mechanische Kombinationen aus Pumpe und regelbarem Motor. Sie arbeiten ohne bewegliche Teile und bestehen im wesentlichen aus einem keramischen Flachkanal mit darübergeschobenem Drehstromständer, der ein magnetisches Wanderfeld erzeugt und damit das flüssige Metall berührungslos durch den Kanal fördert.

Elektromagnetische Pumpen werden in offener Bauweise (Fluctostat®) und in gekapselter Bauweise (Dynoflux®) hergestellt.

Dynoflux®-Pumpen sind in keramischen Tauchgehäusen aufgehängt und somit gegen direkte Metallberührung geschützt.

Electromagnetic induction pumps replace conventional mechanical combinations of pump and controllable motor. They work without movable parts and essentially consist of an ceramic double tube with a sleeve-type three-phase current stator. This generates a magnetic travelling wave which permits contactless transport of the liquid metal through the pump gap.

Electromagnetic pumps can be build in open design (Fluctostat®) or in encased design (Dynoflux®).

Dynoflux® pumps are suspended in ceramic immersion casings which protect them against direct metal contact.

Siemens Energieerzeugung

Anwendungen

Die Flüssigmetallpumpe eignet sich besonders

- zur Badumwälzung,
- zur Behälterumfüllung,
- zum Massel- und Stranggießen und
- zur Metallreinigung

und ist überall dort einsetzbar, wo bei kleinen Druckdifferenzen größere Mengen Metall befördert werden.

Application

The liquid metal pump is primarily suitable for

- bath circulation,
- furnace emptying,
- for continuous and pig mould casting,
- for metal cleaning

and in all cases where large quantities of metal are transported at small pressure differences.

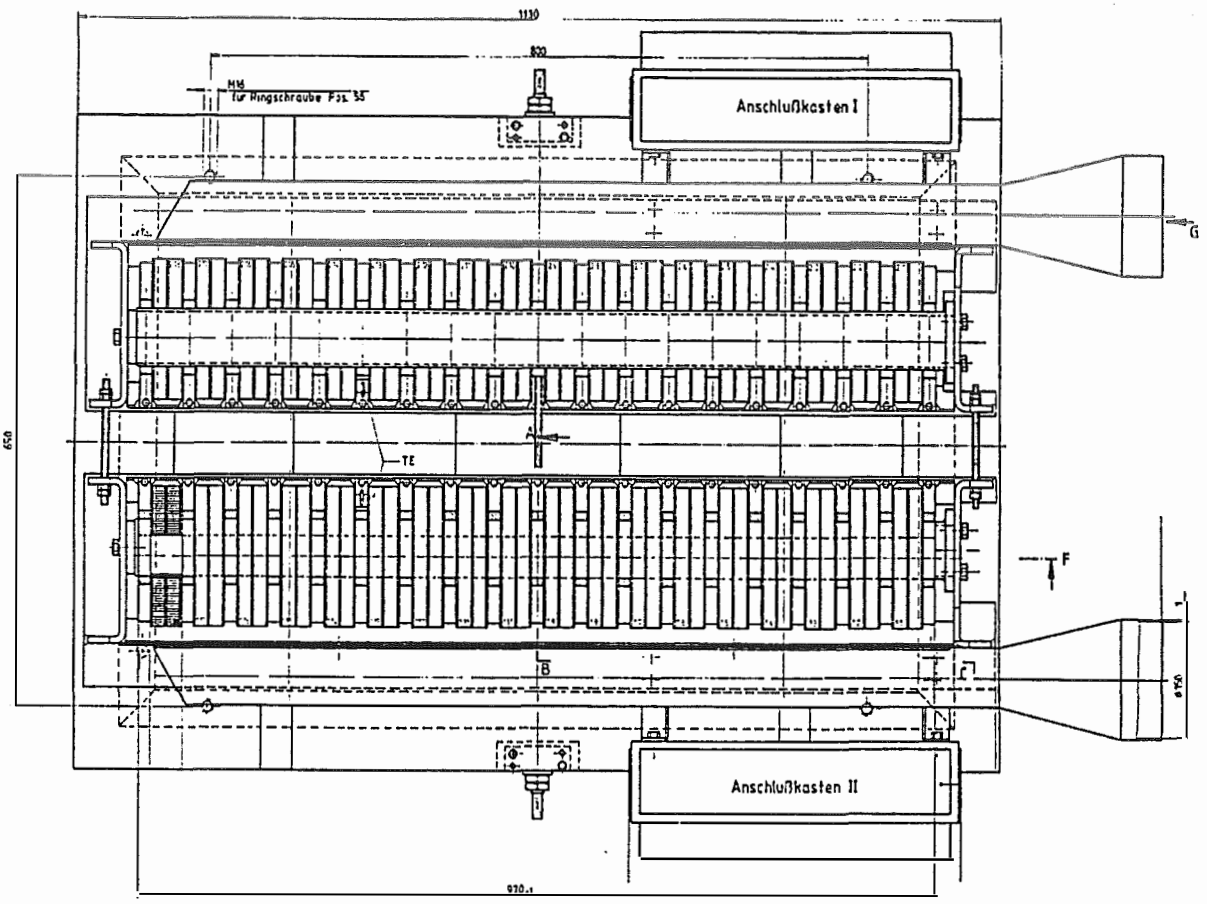

Abmessungen der Z19 K150 Fluctostat

Dimensions of Z19 K150 Fluctostat

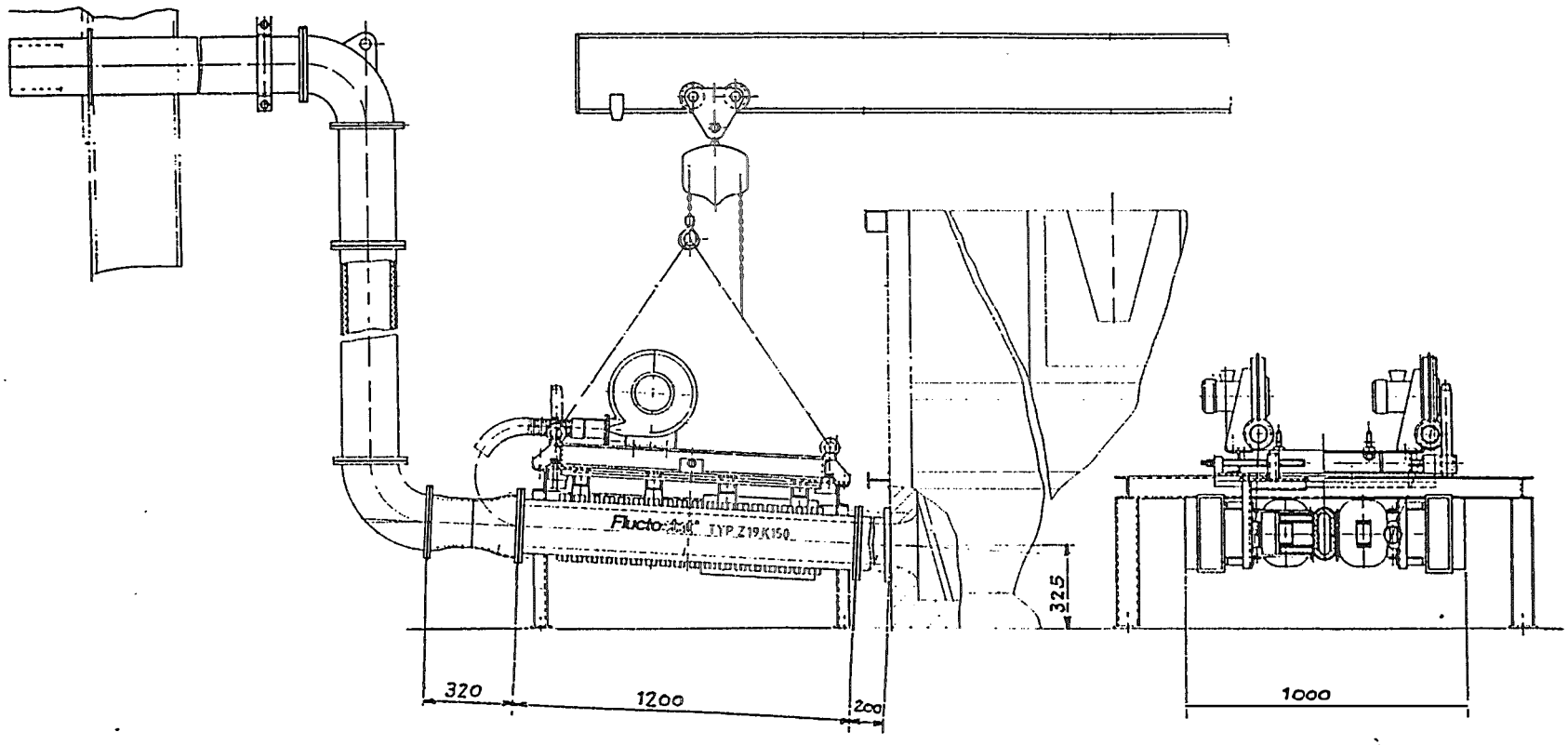

Beispiel: Betrieb einer Z19 K150 Fluctostat in einer Umwälz- und Reinigungsanlage

Example: Application of Z19 K150 Fluctostat in circulation and cleaning facility

Schneckenförderer für

Granulat aus keramischen Werkstoffen

(z.B. SiC und B_4C)

Kh / 10. 1. 1994

Kreislauf
mit SiC- oder B_4C-Granulat

Vergleich der Materialeigenschaften für Al, SiC und B_4C

	ρ	λ		c_p		T_m
	t/m³	W/mK		J/kg K		°C
		300 K	1300 K	300 K	1300 K	
Al	2,7	237	115	900	1100	660
B_4C	2,51	25	14	961		2350
SiC	3,22	100	37	711		2500 subl.

Für SiC wird ein ähnlich großer Volumenstrom wie im Fall von Aluminium angenommen.

Für die Umwälzung des Granulats kommen Schneckenförderer in Frage.

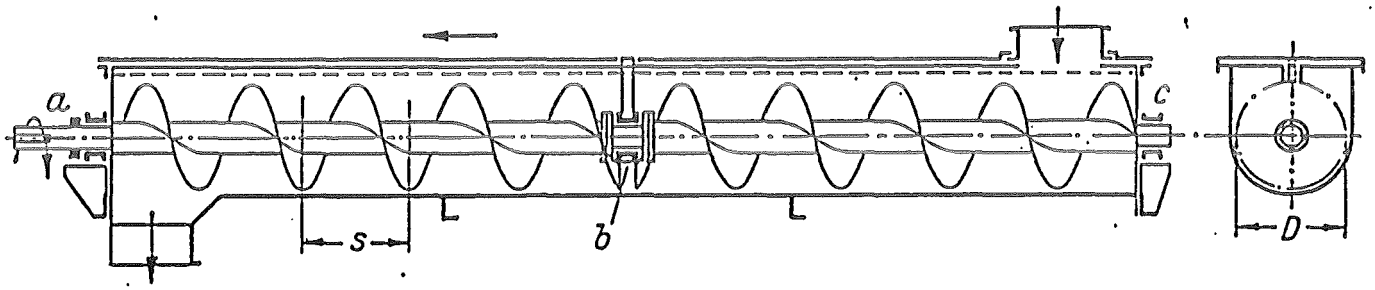

Schneckenförderer mit Vollschnecke. *a* Antriebslager (für Radial- und Axiallast); *b* Zwischenlager (pendelnd); *c* Endlager (für Radiallast)

Auslegung eines Schneckenförderers für einen Volumenstrom von 40 m³/h

$$V = D^2\pi/4 \; x s x \varphi x 60 x n$$

V = Volumenstrom [m³/h] gewählt: 40
D = Schneckendurchmesser [m]
s = Schneckensteigung [m] gewählt: 0,4
φ = Füllungsgrad [-] = 0,15 bei stark schleißendem Fördergut (max. 0,45 bei nicht schleißendem Fördergut)
n = Drehzahl [U/min] gewählt: 60

Dann ergibt sich ein Schneckendurchmesser von 0,5 [m]

Kh / 10. 1. 1994

Erste Informationen aus der Industrie über Schneckenförderer

Elektroschmelzwerk Kempten GmbH

- Hersteller von u.a. B_4C - Granulat bis Körnung 3 mm
- Haben Schneckenförderer aus Metall in Gebrauch zum Fördern von B_4C - Pulver, das sich in einer Suspension befindet.
  Trotzdem große Probleme mit Verschleiß!
- Versuchen z.Z., Schnecke und Rohrinnenwand mit SiC beschichten zu lassen, um Verschleiß zu mindern.
- In unserem Anwendungsfall empfehlen sie, alle Verschleißflächen mit B_4C - oder SiC - Platten zu beplanken. Neuland!
- In unserem Fall muß Aggregat unter Hochvakuum arbeiten. Neuland!
- In unserem Fall Verbesserung des Füllungsgrads (trotz trockenen und stark abrasiven Fördergutes)? Neuland!

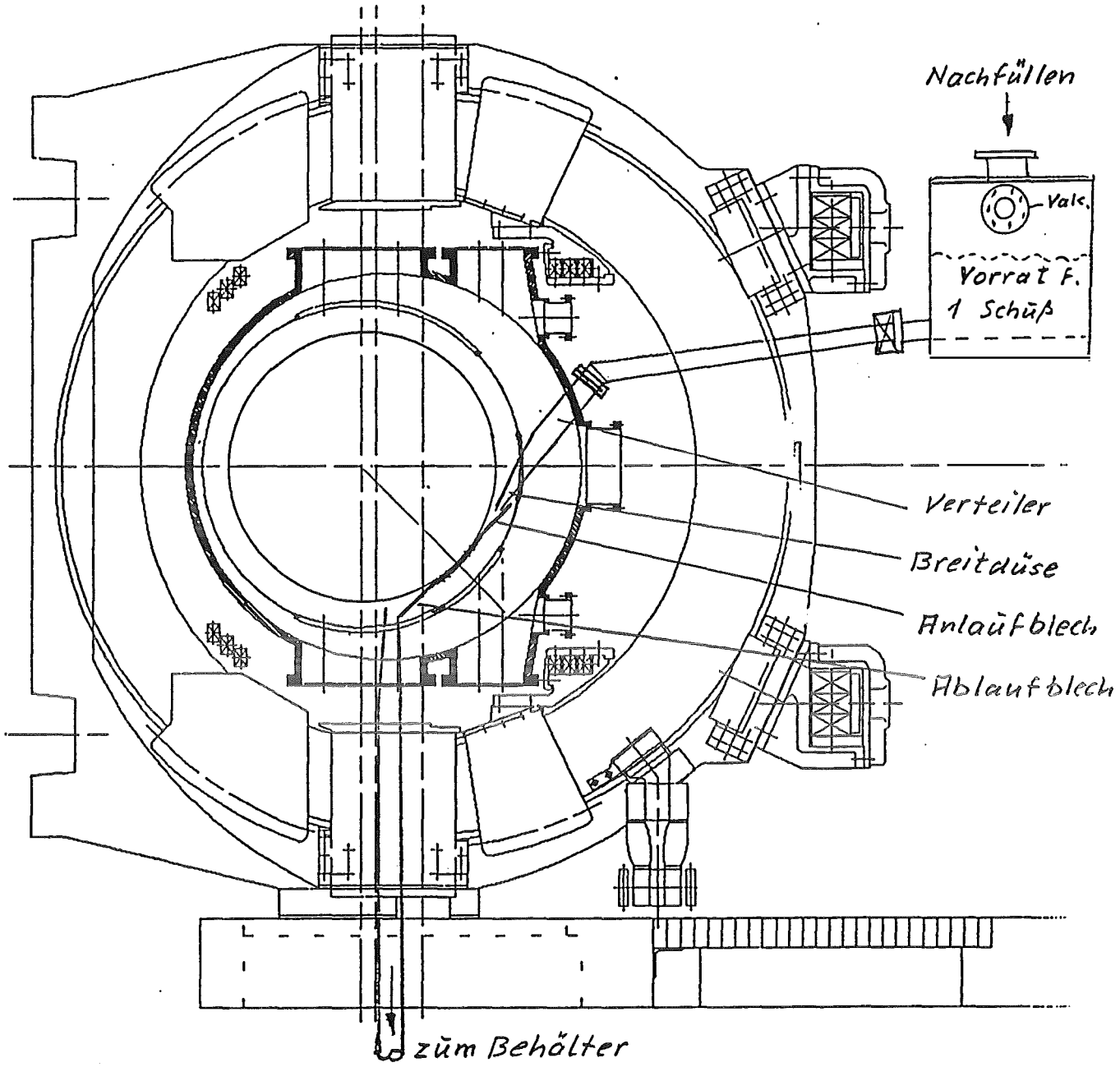

Experiment in TEXTOR

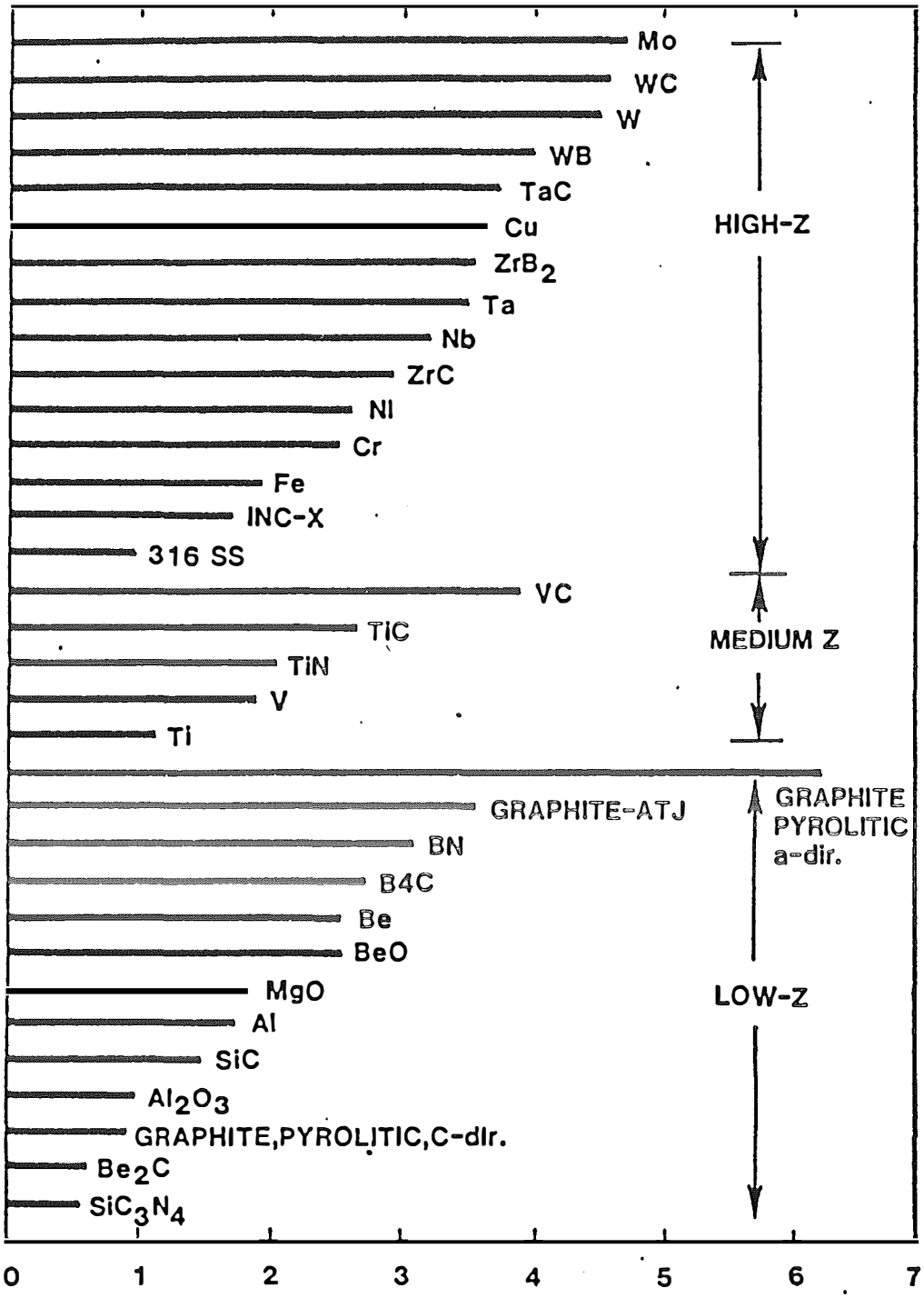

HEAT CAPACITY FIGURE-OF-MERIT $(T_m - T_o)\sqrt{\rho C_p K}$ KJ/cm $^2\sqrt{\text{sec}}$

The transient heating figure-of-merit. Larger numbers imply that more heat can be absorbed in a given amount of time without melting.

9. Conclusions and recommendations (J. Winter)

The discussions of the study group and the analysis of particular aspects presented in this report have led to the following preliminary conclusions:

Although a flow of liquid metals offers the most appealing potential advantages, their use is strongly impeded by the interaction of induced currents and the magnetic field. Even in the absence of transient phenomena, which would tend to make the situation even worse, the motion of a metal through an inhomogeneous magnetic field will lead to intolerable forces, destabilizing the metal flow. This condition exists for a limiter configuration per definition because the limiter intersects the spatially varying poloidal field. In case of a divertor this condition may be slightly relaxed. However Raleigh-Taylor instabilities may be excited leading to ejection of small droplets.

A first analysis of droplets instead of large area liquid metal units shows that these would essentially retain their form if they are small enough, i.e. below a diameter of about 6mm. This is conssitent with experiments made in Russia.

Using a toroidally continuous liquid metal pool at the bottom of the torus with a thickness of the liquid of 1cm would, in the case of TEXTOR, lead to a lifting of the liquid out of the trough. A current is induced by the loop voltage in the liquid which would be attracted by the current in the plasma. The incorporation of breaks would be required leading to leading-edge problems. In addition, a rapid stirring of the liquid would be required for handling large power loads of 50 MWm^{-2}. The useful thickness of Al, assuming heat conduction only, is of the order of 1mm.

The case of a stellarator has been discussed briefly. Due to the absence of a net plasma current all transient phenomena are less important than in a tokamak. The influence of internal exchange currents in the plasma and the concrete geometry of the field lines at the plasma periphery still has to be assessed.

The analysis suggests that a droplet limiter/divertor is probably the most promising configuration when using a liquid metal. Preliminary tokamak experiments were carried out in Russia and it appears to be worthwhile to pursue these experiments in a larger device.

Preliminary analysis of materials compatibility shows that low operation temperatures, in particular at the sensitive pumping elements should be used. This favors e.g. gallium over aluminum.

Unfortunately no electrically insulating liquid with adequate thermal

properties could be found. A rough analysis for low vapour pressure silicon oil (from diffusion pumps) shows that the slow penetration of the heat wave causes very high surface termperature very rapidely. Assuming a tolerable ΔT of 200°C in order to maintain a low vapour pressure, flow velocities of several 100 ms^{-1} would result.

Moving solid balls or spheres suffer from very high stress induced by the rapid heating while moving through the high heat flux zone. These stresses are in excess of the material strength for ceramics (SiC). Assuming that 1 sphere of SiC of 1 cm diameter can accommodate roughly 0.25 kWs while moving with 1 ms^{-1} through the high heat load zone and being heated thereby to about 1400 °C, a turnaround of about 10^6 balls per second would be required to remove 200 MW in ITER. Since the heat removal from the spheres is probably ineffective and will require a long transit time in cool parts of the fusion device, the inventory of spheres will probably be at least a factor of 10 higher. This large number of elements and their integrity is of concern.

The technology exists presently to pump and transport liquid metals at high temperature. The pumps used however have a very low efficiency and consume large powers. To pump even the small amount of liquid metal which would be required for an TEXTOR experiment requires about 350 kW. Conveying the highly abrasive ceramics SiC and B_4C poses serious wear problems in the conveying systems.

The general problem associated with the solid spheres and with liquids comes from the poor penetration of the heat wave, the high associated surface temperatures and the need for high flow velocities if excessive vaporization has to be avoided. The concepts using solid spheres suffer in addition from the large induced stresses.

Two approaches were discussed using rotating drum or wheels. In one case the heat extraction is accomplished through intensive coaxial cooling using a liquid metal as heat transfer and "bearing" medium to a stationary water cooled tube. Stresses and fatigue still could be a problem, even if the CFC's are used. The other proposal is to heat up pyrolytic graphite elements, attached to a rotating wheel, to very high temperatures at which radiation cooling is effective. The temperature excursion of an element during the passage trough the high heat flux zone would be significantly less than in the other cases. These two proposals warrant a more thorough analysis.

It is proposed to host a workshop dedicated to the discussion of fluid targets for heat exhaust in fusion devices during 1995/96 at KFA. Although the topic is sporadically addressed at the major fusion technology conferences, it appears timely to have such a dedicated workshop now. It appears to be useful to invite the leading scientists ad personam to attend

such a workshop. The international know-how could thus be reviewed and made available. Based on the results of this workshop a discussion of the future KFA strategy should be conducted.

10. Relevant literature

The literature listed below is by no means complete but may serve as introduction into the problems.

Journal papers

T.N. Aitov, A.B. Ivanov, and A.V. Tananaev
FLOW OF LIQUID METAL IN A CHUTE IN A COPLANAR MAGNETIC FIELD
Magnetohydrodynamics, A Translation of Magnitnaya Gidrodinamika, 23 (1987) 78

H. Hashizume, Y. Yoshida, K. Miya and K. Ioki
MAGNETOTHERMOHYDRAULIC BEHAVIOR OF THE MOLTEN LAYER OF A FIRST WALL DUE TO PLASMA DISRUPTION
Fusion Engineering and Design **9** (1989) 219-224

A.M. Hassanein, G.L. Kulcinski and W.G. Wolfer
DYNAMICS OF MELTING, EVAPORATION, AND RESOLIDIFICATION OF MATERIALS EXPOSED TO PLASMA DISRUPTIONS
Journal of Nuclear Materials **111&112** (1982) 554-559

P. Jung
DIFFUSION AND RETENTION OF HELIUM IN GRAPHITE AND SILICON CARBIDE
Journal of Nuclear Materials **191-194** (1992) 377-381

C. Liao, M. S. Kazimi and J. E. Meyer
ON HYDROGEN TRANSPORT AND EDGE PLASMA MODELING OF LIQUID-METAL DIVERTORS
Fusion Technology **23** (1993) 208

C. Liao, M. S. Kazimi
A FEASIBILITY ASSESSMENT OF LIQUID METAL DIVERTORS
Fusion Technology **21** (1992) 1845

C. Liao, B. LaBombard, B. Lane, M. S. Kazimi
ON MODELING OF PLASMA EDGE CONDITIONS AT DIVERTORS WITH SOLID METAL NEUTRALIZERS
Fusion Technology **21** (1992) 41

S.V. Mirnov, V.N. Dem'yanenko, E.V. Murav'ev
LIQUID-METAL TOKAMAK DIVERTORS
Journal of Nuclear Materials **196-198** (1992) 45-49

Th. K.R. Richter
CHEMICAL SPUTTERING ASPECTS OF LIQUID METAL FILM DIVERTOR TARGETS IN NUCLEAR FUSION DEVICES
Journal of Nuclear Materials **183** (1991) 216

T. Uchikawa, A. Miyahara
DESIGN AND FABRICATION OF THE ALT-II LIMITER BLADES
Fusion Engineering and Design **13** (1990) 283-289

K. Takase, M.Z. Hasan and T. Kunugi
NON MHD LAMINAR FLOW
Fusion Technology **21** (1992) 1841

V.O. Vodyanyuk, V.N. Dem'yanenko, A. F. Kolesnichenko, S.V. Mirnov, E.V. Murav'ev, E.K. Sergeev, and A.M. Shapiro
LIQUID-METAL TOKAMAK LIMITER: STATEMENT OF THE PROBLEM AND FIRST RESULTS
Sov. J. Plasma Phys. **14(5)** (1988) 370

J.B. Whitley
MATERIAL CONSIDEREATIONS FOR HIGH HEAT FLUX COMPONENTS
Journal of Nuclear Materials **133&134** (1985) 39-45

W.G. Wolfer and A.M. Hassanein
ON MELT LAYER STABILITY FOLLOWING A PLASMA DISRUPTION
Journal of Nuclear Materials **111&112** (1982) 560-565

Reports

ABOUT THE ITER DIVERTOR CONCEPT
V.I. Pistunovich, Kurchatov Institute Moscow, Russia
Technical Meeting and Workshop on ITER Divertor Physics and Design, Garching, 21. - 25. February, 1994

PROPERTIES OF MATERIALS
M.F. Smith and J.B. Whitley, Sandia National Laboratories Albuquerque, NATO Advanced Study Institute on the Physics of Plasma-Wall Interactions in Controlled Fusion,
Val-Morin, Canada, 30 July - 10 August 1984

EIN FLÜSSIGMETAL-FILM-DIVERTOR ALS ALTERNATIVE FÜR FUSIONSREAKTOREN DER NÄCHSTEN GENERATION
Dr. G. Class, Kernforschungszentrum Karlruhe, Institut für Reatorentwicklung,
Forschungszentrum Jülich GmbH, Institut für Reaktorentwicklung, 25.10.1990

ÜBERLEGUNGEN ZUR WECHSELWIRKUNG ZWISCHEN DEM SCRAPE OFF LAYER EINES TOKAMAKPLASMAS MIT EINER FLÜSSIGMETALL DIVERTORPLATTE
R. Klingelhöfer, Kernforschungszentrum Karlsruhe,
Primärbericht 03.00.01 P 12A, November 1991

IAEA TECHNICAL REPORT,
IAEA-TECDOC-373, INTOR
(1986), P1.1 - P 1.16

IMPURITY CONTROL
FIRST WALL, BLANKET
I.V. Mazul
USSR Contribution to INTOR Workshop Phase IIA, Part 3, 1987

Report of the Review Panel on the Division of Development & Technology Workshop on
INNOVATIVE TECHNOLOGIES FOR IMPURITIES CONTROL
R.E. Nygren (Ed.)
Sandia National Laboratories, Albuquerque, New Mexico 87185, SAND91-0029,
March 1992